석 사 학 위 논 문

Master's Thesis

다항식 강화 기법이 적용된 확장유한요소법을 이용한 2차원 균열 해석

Two-dimensional crack analysis using the extended finite element method with polynomial enrichment technique

2018

김 기 환 (金 起 煥 Kim, Gihwan)

한 국 과 학 기 술 원

Korea Advanced Institute of Science and Technology

석 사 학 위 논 문

다항식 강화 기법이 적용된 확장유한요소법을 이용한 2차원 균열 해석

2018

김 기 환

한 국 과 학 기 술 원

기계공학과

다항식 강화 기법이 적용된 확장유한요소법을 이용한 2차원 균열 해석

김 기 환

위 논문은 한국과학기술원 석사학위논문으로
학위논문 심사위원회의 심사를 통과하였음

2017년 12월 13일

심사위원장 이 필 승 (인)

심 사 위 원 윤 정 환 (인)

심 사 위 원 유 승 화 (인)

Two-dimensional crack analysis using the extended finite element method with polynomial enrichment technique

Gihwan Kim

Advisor: Phill-Seung Lee

A thesis submitted to the faculty of
Korea Advanced Institute of Science and Technology in
partial fulfillment of the requirements for the degree of
Master of Science in Mechanical Engineering

Daejeon, Korea
December 13, 2017

Approved by

Phill-Seung Lee
Professor of Mechanical Engineering

The study was conducted in accordance with Code of Research Ethics[1)].

1) Declaration of Ethical Conduct in Research**:** I, as a graduate student of Korea Advanced Institute of Science and Technology, hereby declare that I have not committed any act that may damage the credibility of my research. This includes, but is not limited to, falsification, thesis written by someone else, distortion of research findings, and plagiarism. I confirm that my dissertation contains honest conclusions based on my own careful research under the guidance of my advisor.

MME
20163067

김기환. 다항식 강화 기법이 적용된 확장유한요소법을 이용한 2차원 균열 해석. 기계공학과. 2018년. 61+v 쪽. 지도교수: 이필승. (영문 논문)

Gihwan Kim. Two-dimensional crack analysis using the extended finite element method with polynomial enrichment technique. Department of Mechanical Engineering. 2018. 61+v pages. Advisor: Phill-Seung Lee. (Text in English)

초 록

확장유한요소법/일반유한요소법은 균열을 해석하기 위해 가장 많이 쓰이는 방법 중 하나이다. 이 방법은, 단위분할법을 이용하여 변위장을 풍부하게 하여 균열진전시에, 격자 재구성을 할 필요 없는 방법이다. 그러나, 만족하는 해를 얻기 위해서는 균열 선단 근처의 메쉬 세분화 과정은 여전히 필요하다. 최근에, 2차원 사각 요소에서 선형 종속 문제를 해결하고 다항식 강화 기법을 통해 해를 개선시키는 연구가 제시되었다. 본 학위논문에서는 기존의 2차원 사각 요소를 이용해 확장유한요소법에 선형 종속 문제를 해결한 다항식 강화 기법이 적용되었다. 이로 인해, 메쉬 세분화 과정이 필요하지 않는 방법이 제안되었다. 또한, Zienkiewicz-Zhu 오차 추정기를 통해 자유도 측면에서 효율적인 적응적 국부 강화 기법이 제안되었다. 제안된 방법의 검증은 여러 파괴역학적 수치 예제를 통해 수행되었다.

핵 심 낱 말 확장유한요소법, 일반유한요소법, 균열해석, 파괴역학, 단위분할법

Abstract

Extended Finite Element Method / General Finite Element Method is one of the most commonly used methods for crack analysis. This method does not require re-meshing as the crack propagates by enriching the displacement field by the partition of unity method. However, the mesh refinement process near the crack tip is still necessary to obtain a satisfactory solution. Recently, research was proposed to solve the linear dependence problem using the 2-D 4-node quadrilateral elements and to improve the solution through polynomial enrichment technique. In this thesis, a polynomial enrichment technique that resolves the linear dependence problem is applied to the Extended Finite Element Method using the 2-D 4-node quadrilateral elements. As a result, a method that does not require a mesh refinement process is proposed. In addition, an efficient adaptive local enrichment technique is proposed through the Zienkiewicz-Zhu error estimator in terms of degrees of freedom. Verification of the proposed method is performed through several fracture mechanics numerical examples.

Keywords XFEM, GFEM, crack analysis, fracture mechanics, partition of unity

Contents

List of Tables

List of Figures

Chapter 1. Introduction

1.1 Research Background

The finite element method (FEM) has been applied to aerospace and aerospace engineering, automotive industry, mechanical engineering, civil engineering, biomechanics, geomorphology, and materials science since it is more powerful and effective in solving problems than other methods [1]. FEM has also been widely applied in linear elastic fracture mechanics. However, the mesh is dependent on the geometry of the crack, and in order to obtain an accurate solution with FEM re-meshing is necessary when the crack progresses and is time-consuming. In addition, if you use standard elements, you need mesh refinement around the crack tip.

The partition of unity method was first introduced by Melenk, J. M., and Babuška [2], and various partition of unity based methods have been proposed [3-6] and the extended finite element method or general finite element method (XFEM / GFEM) has been proposed [7-10]. The basic concept of XFEM / GFEM is to enrich the finite element analysis space by using the partition of unity. XFEM and GFEM are essentially the same method, and in this paper two words are used in combination. XFEM was first introduced by Belytschko and Black [7] and further developed by Moës et al. [11]. This method is a method of modeling cracks by enriching the finite element analysis space using the Heaviside step function and the asymptotic crack tip function as the enrichment function in the element including the displacement discontinuity. This makes it possible to construct the mesh geometry independently of the geometry of the crack, so that re-meshing becomes unnecessary.

It has been found that even though XFEM presents a very accurate solution in fracture mechanics analysis, the convergence rate is not optimized for the element size and the solution is not improved as the polynomial order of interpolation increases [12]. This shows that the singularity of the crack tip defined by the asymptotic field is not well captured.

Laborde et al. [13] and Béchet et al. [14] proposed the use of enrichment in specific areas around the crack tip, independent of element size. This method is called geometrical enrichment. This method greatly improves the convergence with respect to the element size, but increases the condition number of the global stiffness matrix to make the global matrix into an ill-condition matrix. Thus, there is a need for a method of obtaining a high-accuracy solution with minimal enrichment.

1.2 Research Purpose

In this paper, we aim to apply a polynomial enrichment technique to standard XFEM to improve the solution without mesh refinement around the crack tips using 2D 4-node quadrilateral elements. In addition, in order to obtain a solution with a high accuracy by applying a minimum enrichment, the goal is to obtain an adaptive local enrichment strategy and a better solution than XFEM with geometrical enrichment.

Chapter 2. Fracture Mechanics

2.1 Linear Elastic Fracture Mechanics

Fracture mechanics was originally focused on the behavior of elastic materials applied to Hooke's law. By Orowan (1948), Irwin (1957) and Barenblatt (1962), numerous experiments and theories have been presented to represent the behavior of crack regions in linear elastic materials. The concept of LEFM for nonlinear behavior such as plastic behavior was extended by Irwin (1960) and Shih and Hutchinson (1976). The fractured domain leads to a singularity at the stress field in the crack tip region for the elastic material. However, in the case of plastic materials, a plastic zone is generated at the crack tip and the stress reaches a finite value equal to the yield stress of the material.

To investigate the fracture behavior of the material, the researchers performed many microscopic and macroscopic studies. From a microscopic point of view, crack propagation can occur if the potential energy of an atom is greater than the bound energy present between two adjacent atoms.

However, from the macroscopic point of view of continuum mechanics, the modeling of cracks and the growth of cracks can be explained by fracture mechanics. In the following, the basics of LEFM are introduced, such as energy release rate, evaluation of the stress distribution around the crack tip, and the stress intensity factors in different load modes.

2.1.1 Stress distribution in the vicinity of a crack tip

When a load is applied to a cracked mechanical part, it can be seen that the stress concentration due to the area reduction with respect to the nominal area occurs. The crack geometry leads to high stress concentration around the crack tip. This phenomenon is described in detail in Figure 2.1. The plastic zone appears because of the high tension visible at the crack edges. In the case of the majority of brittle materials, the size of the plastic zone is small and the LEFM theory can be applied. According to the LFEM theory, the crack behavior is assumed to be an ideal crack following a linear elastic model without considering the plastic behavior. [15].

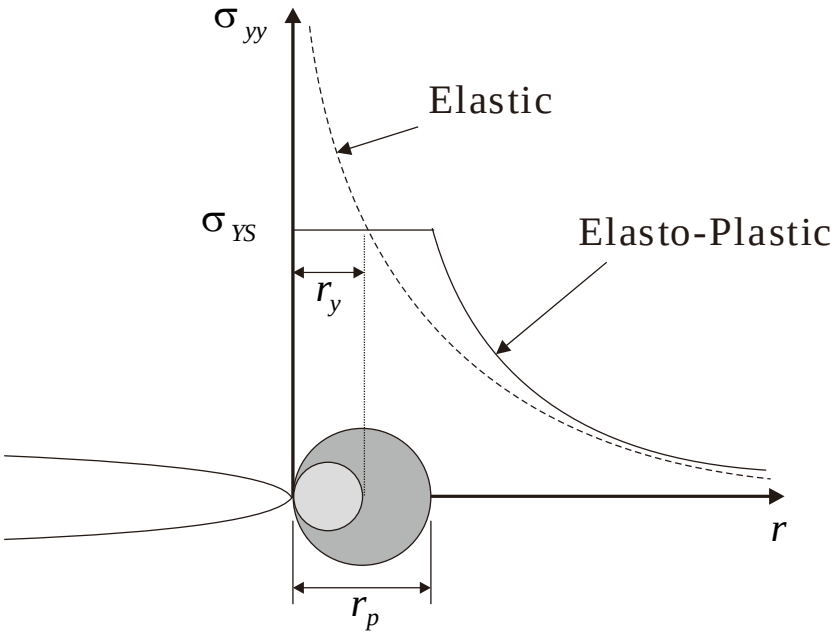

Figure 2.1 Elastic and Elasto-Plastic crack behavior

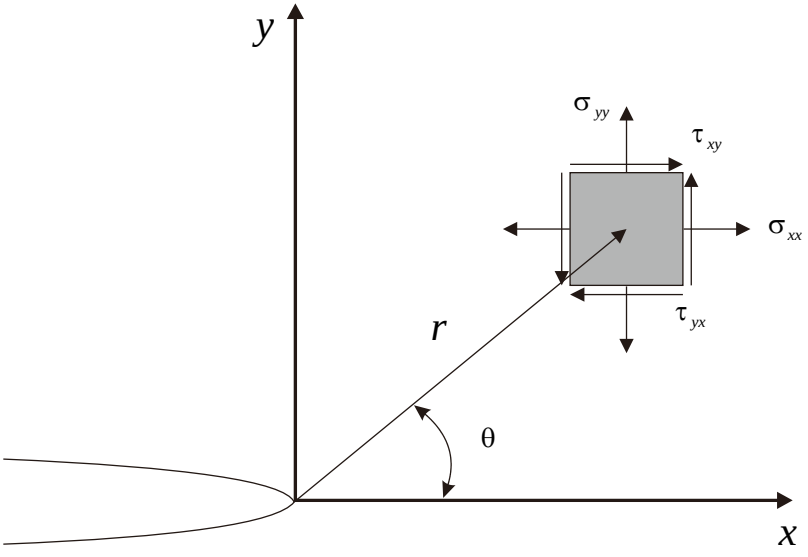

Figure 2.2 Stress componenets around the crack tip and poloar coordinates

Taking into account the polar coordinate system, (r,θ), with the origin of the crack at the origin as shown in Figure 2.2, the stress field around the crack of any linear elastic body can be given by

$$\sigma_{ij} = (\frac{k}{\sqrt{r}}) f_{ij}(\theta) + \sum_{m=0}^{\infty} A_m r^{\frac{m}{2}} g_{ij}^{(m)}(\theta), \tag{2.1}$$

where σ_{ij} is the stress tensor, k is a constant, $f_{ij}(\theta)$ is a dimensionless function and function of θ. Considering the higher order term, A_m is a constant corresponding to the mth term and g_{ij} is a dimensionless function corresponding to the mth term. The above equation is a general stress field around the crack, and we should note that this equation has a leading term proportional to $1/\sqrt{r}$. As r approaches zero, the leading term is close to infinity. However, because of the other higher-order terms approach or near certain finite values, the stress field is dominated by the leading term. Therefore, the stress near the crack tip varies of $1/\sqrt{r}$ independently of the geometry and loading.

2.1.2 The Griffith energy balance

When the system changes from non-equilibrium to equilibrium, the net energy of the system decreases according to the first thermodynamic law. Griffith applied this concept to the mechanism of crack formation in 1920 [15, 16].

Only when certain processes reduce the total energy or remain constant, cracks can be formed or existing cracks can grow. Therefore, we can define the critical condition for fracture as the point at which the crack grows in the equilibrium state without changing net energy in the total energy.

Consider a wide plate with crack length $2a$ under a constant stress σ shown in Figure 2.3. Sufficient potential energy that exceeds the surface energy γ_s of the material is required to increase the length of the crack. In an equilibrium state, the Griffith energy balance is given by

$$\frac{dE}{dA} = \frac{dW_s}{dA} + \frac{d\Pi}{dA} = 0, \tag{2.3}$$

Or

$$\frac{d\Pi}{dA} = -\frac{dW_s}{dA}, \tag{2.4}$$

where A is the crack area, E is the total energy, Π is the potential energy supplied by the internal strain energy and external forces and W_s is the work needed to generate new surfaces.

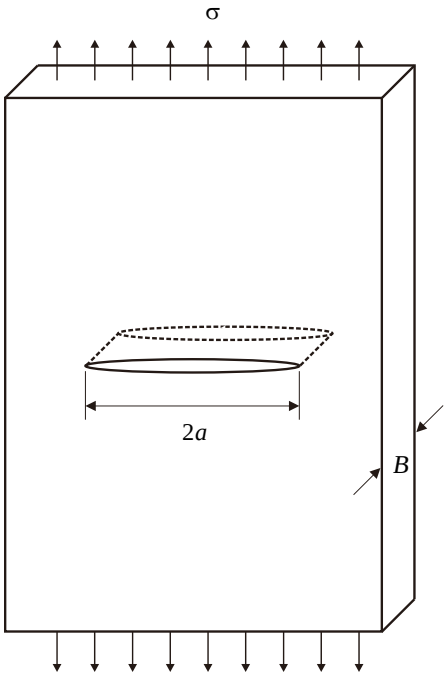

Figure 2.3 Central crack in an infinite plate with thickness under tensile stress

For the plate with the crack shown in Figure 2.3, Griffith proposed the following equation using the stress analysis of Inglis [17].

$$\Pi = \Pi_0 - \frac{\pi a^2 B \sigma^2}{E}, \tag{2.5}$$

where Π_0 is the potential energy of a plate without cracks, B is the thickness of the plate. For the formation of the crack, it is necessary to create two surfaces, W_s is as follows

$$W_s = 4\gamma_s aB, \tag{2.6}$$

in which γ_s is the surface energy of the material.

Thus, by Equation (2.4) and Equation (2.5), following equation is obtained

$$-\frac{d\Pi}{dA} = \frac{\pi a \sigma^2}{E}. \tag{2.7}$$

And, substituting W_s in Equation (2.6) into Equation (2.4), the following equation is obtained

$$\frac{dW_s}{dA} = 2\gamma_s. \tag{2.8}$$

Using the above equations to obtain the fracture stress, the following equation is obtained

$$\sigma_f = \sqrt{\frac{2E\gamma_s}{\pi a}}. \tag{2.9}$$

The difference between the crack area and the surface area should be clearly understood. In Figure 2.3,

the surface area is $2A$. However, the crack area defined as the projected area of the crack is $2aB$.

2.2.3 Energy release rate

An energy approach essentially equivalent to Griffith's model was proposed by Irwin [18] in 1956. Irwin's method is more convenient for dealing with engineering problems. An energy release rate G defined by Irwin is a measure of the energy available for an increment of crack extension and defined as [15]

$$G = -\frac{d\Pi}{dA}. \tag{2.10}$$

In the previous context, at the energy release rate, the term rate is not mean a derivative with respect to time. The energy release rate G is the rate of change in potential energy Π with the crack area A. G is called crack driving force or crack extension force since it is obtained from the derivative of the potential with respect to crack area. By substituting Equation (2.10) into the right-hand side of Equation (2.7), the energy release rate for the wide plate with crack length $2a$ in the plane stress (Figure 2.3) is given by

$$G = \frac{\pi a \sigma^2}{E}. \tag{2.11}$$

In the previous section, when G reaches a critical value, crack extension occurs, i.e.,

$$G_c = \frac{dW_s}{dA} = 2w_f, \tag{2.12}$$

where G_c is a critical value of an energy release rate and a measure of the fracture toughness of the material.

2.2.4 Three loading modes

In fracture mechanics, there are basically three types of fracture, Mode I, Mode II and Mode III. The three modes are schematically shown in Figure 2.4.

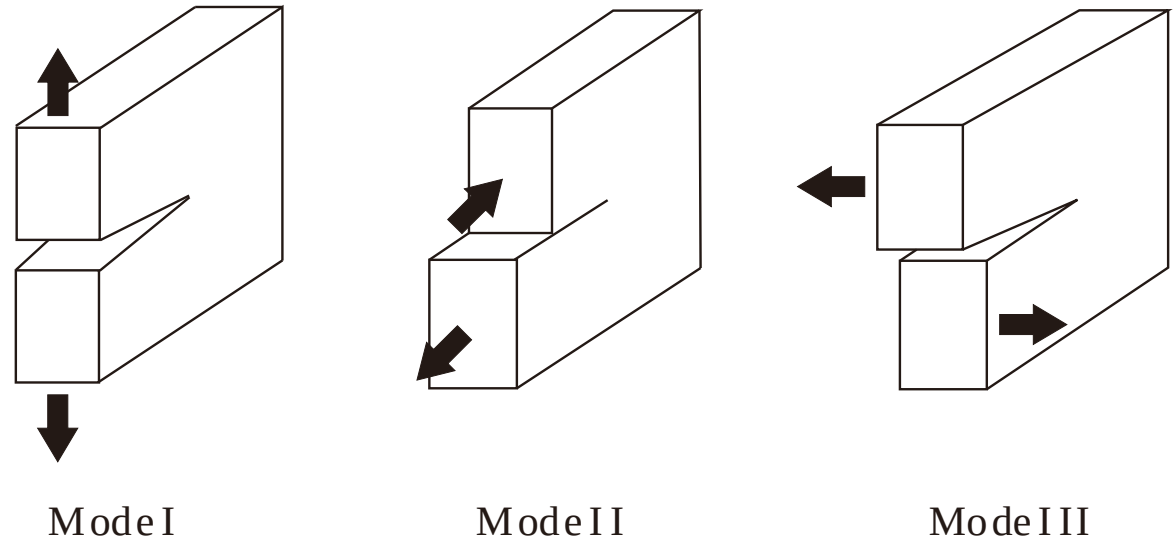

Figure 2.4 Loading modes (Mode I, Mode II and Mode III)

Mode I is called the opening mode and refers to the failure mode in which the tensile load is applied perpendicular to the crack plane (a traction mode).

Mode II is called in-plane shear / sliding mode and refers to a failure mode in which the shear stress is parallel to the crack plane and acting perpendicular to the crack front (a shear mode).

Mode III, called the out-of-plane tear mode, refers to a failure mode in which shear stress acts parallel to cracks and crack fronts (a torsion mode).

2.2.5 Stress intensity factor

Under the assumption of linear elastic behavior (LEFM), the stress intensity factors can be used as a measure to quantify the severity of cracks relative to other cracks and can be employed to determine the stress, strain and displacement around the crack tip. They are related not only to the mechanism of crack initiation but also to the propagation of cracks, which is a very important measure in studying cracks. When the stress intensity factor reaches the extreme value, it causes component failure. The extreme value at this point is called fracture toughness K_c .

When the above three load modes are applied, the crack tip will have a singularity of $1/r$, and the proportional constants k and f_{ij} vary depending on the mode. At this point, it is recommended to replace k in

Equation (2.1) with a stress intensity factor K where $K = k\sqrt{2\pi}$. The stress intensity factor is generally expressed as K_I , K_{II} or K_{III} depending on the load mode. Furthermore, under the assumption that the material is isotropic and linear elastic, the stress fields around the crack tip can be written as

$$\lim_{r\to 0} \sigma_{ij}^{(I)} = \frac{K_I}{\sqrt{2\pi r}} f_{ij}^{(I)}(\theta), \tag{2.13}$$

$$\lim_{r\to 0} \sigma_{ij}^{(II)} = \frac{K_{II}}{\sqrt{2\pi r}} f_{ij}^{(II)}(\theta), \tag{2.14}$$

$$\lim_{r\to 0} \sigma_{ij}^{(III)} = \frac{K_{III}}{\sqrt{2\pi r}} f_{ij}^{(III)}(\theta), \tag{2.15}$$

for mode I, mode II and mode III.

If there is no body force and traction-free boundary conditions at the crack faces are applied and higher order terms are ignored, the stress around the crack tip for mode I loading can be obtained as

$$\sigma_{xx} = \frac{K_I}{\sqrt{2\pi r}} \cos\frac{\theta}{2}\left(1 - \sin\frac{\theta}{2}\sin\frac{3\theta}{2}\right), \tag{2.16}$$

$$\sigma_{yy} = \frac{K_I}{\sqrt{2\pi r}} \cos\frac{\theta}{2}\left(1 + \sin\frac{\theta}{2}\sin\frac{3\theta}{2}\right), \tag{2.17}$$

$$\tau_{xy} = \frac{K_I}{\sqrt{2\pi r}} \sin\frac{\theta}{2}\cos\frac{\theta}{2}\cos\frac{3\theta}{2}, \tag{2.18}$$

$$\sigma_{zz} = \begin{cases} \nu(\sigma_{xx} + \sigma_{yy}) & for \quad plane\ strain \\ 0 & for \quad plane\ stress \end{cases}, \tag{2.19}$$

$$\tau_{yz} = 0, \ \ \tau_{zx} = 0, \tag{2.20}$$

and the displacement fields as

$$u_x = \frac{K_I(1+\nu)}{E}\sqrt{\frac{r}{2\pi}} \cos\frac{\theta}{2}\left(\kappa - 1 + 2\sin^2\frac{\theta}{2}\right), \tag{2.21}$$

$$u_y = \frac{K_I(1+\nu)}{E}\sqrt{\frac{r}{2\pi}} \sin\frac{\theta}{2}\left(\kappa - 1 - 2\cos^2\frac{\theta}{2}\right), \tag{2.22}$$

$$u_z = 0, \tag{2.23}$$

where ν is the Poisson ratio, E is the elastic modulus, $\kappa = 3 - 4\nu$ for plane strain and $\kappa = \frac{3-\nu}{1+\nu}$ for plane stress.

In mode II loading, the stress fields around the crack tip are obtained as

$$\sigma_{xx} = -\frac{K_{II}}{\sqrt{2\pi r}} \sin\frac{\theta}{2}\left(2 + \cos\frac{\theta}{2}\cos\frac{3\theta}{2}\right), \tag{2.24}$$

$$\sigma_{yy} = \frac{K_{II}}{\sqrt{2\pi r}} \sin\frac{\theta}{2}\cos\frac{\theta}{2}\cos\frac{3\theta}{2}, \tag{2.25}$$

$$\tau_{xy} = \frac{K_{II}}{\sqrt{2\pi r}} \cos\frac{\theta}{2}\left(1 - \sin\frac{\theta}{2}\sin\frac{3\theta}{2}\right), \tag{2.26}$$

$$\sigma_{zz} = \nu(\sigma_{xx} + \sigma_{yy}), \tag{2.27}$$

$$\tau_{yz} = 0, \quad \tau_{zx} = 0, \tag{2.28}$$

and the displacement fields as

$$u_x = \frac{K_{II}(1+\nu)}{E}\sqrt{\frac{r}{2\pi}} \sin\frac{\theta}{2}\left(\kappa + 1 + 2\cos^2\frac{\theta}{2}\right), \tag{2.29}$$

$$u_y = -\frac{K_{II}(1+\nu)}{E}\sqrt{\frac{r}{2\pi}} \cos\frac{\theta}{2}\left(\kappa - 1 - 2\sin^2\frac{\theta}{2}\right), \tag{2.30}$$

$$u_z = 0, \tag{2.31}$$

in which ν is the Poisson ratio, E is Young's modulus, $\kappa = 3 - 4\nu$ for plane strain and $\kappa = \frac{3-\nu}{1+\nu}$ for plane stress.

In mode III loading, the stress fields around the crack tip are obtained as

$$\tau_{yz} = \frac{K_{III}}{\sqrt{2\pi r}} \cos\frac{\theta}{2}, \tag{2.32}$$

$$\tau_{zx} = -\frac{K_{III}}{\sqrt{2\pi r}} \sin\frac{\theta}{2}, \tag{2.33}$$

$$\sigma_{xx} = 0, \quad \sigma_{yy} = 0, \quad \sigma_{zz} = 0, \quad \tau_{xy} = 0, \tag{2.34}$$

and the displacement fields as

$$u_z = \frac{K_{III}(1+\nu)}{E}\sqrt{\frac{r}{2\pi}} \sin\frac{\theta}{2}, \tag{2.35}$$

$$u_x = 0, \quad u_y = 0, \tag{2.36}$$

where ν is the Poisson ratio, E is Young's modulus.

In a mixed-mode problem, the total stress and displacement fields from the principle of linear superposition can be obtained as

$$\sigma_{ij}^{(Total)} = \sigma_{ij}^{(I)} + \sigma_{ij}^{(II)} + \sigma_{ij}^{(III)}, \tag{2.37}$$

$$u_i^{(Total)} = u_i^{(I)} + u_i^{(II)} + u_i^{(III)}. \tag{2.38}$$

2.2.6 Relation between energy release rate and stress intensity factor

The energy release rate G of the energy approach and the stress intensity factor K of the stress concentration approach, which are the main parameters of the linear elastic fracture mechanics, may have been independently developed. Many engineers prefer the stress intensity factor approach, but in some cases the energy release rate approach is useful. The relationship between the stress intensity factor K and the release rate G is given by

$$G = \frac{K^2}{E_{eff}}, \tag{2.39}$$

$$E_{eff} = \begin{cases} E & plane\,stress \\ \dfrac{E}{1-\nu^2} & plane\,strain \end{cases}, \tag{2.40}$$

in which ν is the Poisson's ratio and E is the elastic modulus.

2.2 Elasto Plastic Fracture Mechanics

Although the linear elastic fracture mechanics (LEFM) has been able to effectively represent stress fields and displacements near the crack tip, the LEFM theories are applicable only to materials with a linear elastic behavior such as brittle materials. However, there are also ductile materials that do not behave like linear elastic behavior such as steel. In the case of such a ductile material, the plastic zone becomes larger and can no longer be ignored. Therefore, when evaluating the fracture toughness of materials, this plasticity effect must be considered.

2.2.1 J-integral

A method of calculating the energy release rate, the so-called J-integral, was proposed by Rice in the late 1960s [19]. The J-integral represents a method of calculating the energy release rate of nonlinear materials and is also called J-contour integral or conservation integral. This method is a very innovative way to idealize elasto-plastic deformation as nonlinear elastic, which can expand the limit of the linear elastic fracture mechanics. Also, since the J-integral is path-independent, evaluating the J integral in a far field near a crack tip can be related to deformation near the tip.

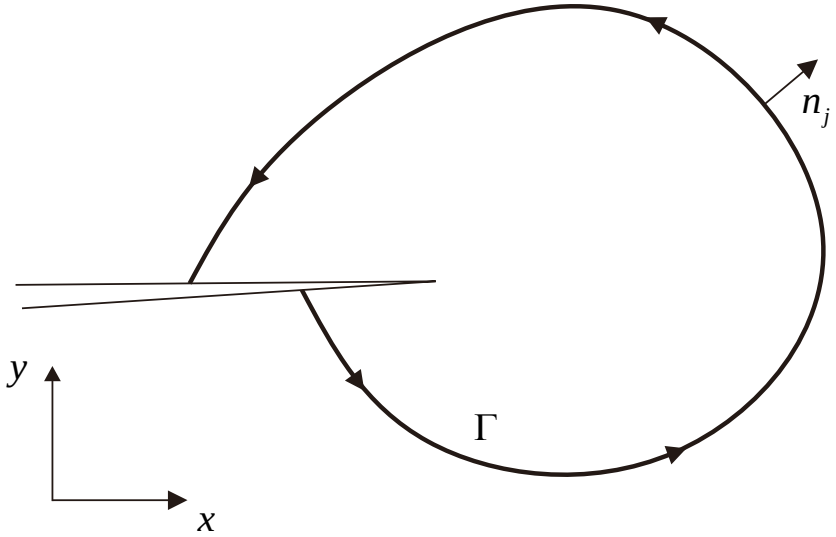

Figure 2.5 J-integral contour around the crack tip

The original form of the integral proposed by Rice is as follows

$$J = \int_{\Gamma} \left(W dy - T_i \frac{\partial u_i}{\partial x} ds \right), \tag{2.41}$$

where u_i is the displacement vector and Γ is a path around the crack tip is the length increment along the contour Γ. The J-integral is evaluated by the path Γ from the lower crack surface to the upper crack surface in a counterclockwise direction. W is the strain energy density given by

$$W = \int_0^{\varepsilon_{ij}} \sigma_{ij} d\varepsilon_{ij}, \tag{2.42}$$

where σ_{ij} is the stress tensor and ε_{ij} is the strain tensor. T_i is the traction vector given by

$$T_i = \sigma_{ij} n_j, \tag{2.43}$$

in which σ_{ij} is the stress tensor and n_j is the unit vector normal to Γ.

Using the Kronecker Delta property, Equation (2.41) can also be written as

$$J = \int_{\Gamma} \left(W\delta_{1j} - \sigma_{ij} \frac{\partial u_i}{\partial x_1} \right) n_j d\Gamma , \tag{2.44}$$

where δ_{1j} is the Kronecker delta.

J is the general form of the energy release rate. Therefore, for nonlinear elastic materials, J is equal to the energy release rate G. we can rewrite Equation (2.39) in terms of mixed-mode fracture as

$$G = J = \frac{K_I{}^2}{E_{eff}} + \frac{K_{II}{}^2}{E_{eff}} , \tag{2.45}$$

$$E_{eff} = \begin{cases} E & plane stress \\ \dfrac{E}{1-\nu^2} & plane strain \end{cases} . \tag{2.46}$$

2.2.2 Interaction integral

In the mixed-mode loading condition, the stress fields and displacements around the crack tip are separated into values corresponding to the respective modes, as in Equation (2.37) and Equation (2.38). When the stress intensity factors K_I and K_{II} are obtained, the stress field and the displacement around the crack tip can be known. To obtain K_I and K_{II}, the auxiliary field method is commonly used [20, 21]. By using this method, the mixed-mode stress intensity factor can be obtained by superimposing the auxiliary stress and displacement state on the FEM stress and displacement solution considering the two states of the crack body. The state (1) given as $\varepsilon_{ij}^{(1)}, \sigma_{ij}^{(1)}$ and $u_{ij}^{(1)}$ represents the actual state, which is obtained by Finite Element Method. The state (2) denoted by $\varepsilon_{ij}^{(2)}, \sigma_{ij}^{(2)}$ and $u_{ij}^{(2)}$ means a state in the asymptotic field for Mode I or Mode II, respectively. By using superposition of state (1) and state (2), Equation (2.44) can be written as follows

$$J^{(1+2)} = \int_{\Gamma} \left[\frac{1}{2} (\sigma_{ij}^{(1)} + \sigma_{ij}^{(2)})(\varepsilon_{ij}^{(1)} + \varepsilon_{ij}^{(2)})\delta_{1j} - (\sigma_{ij}^{(1)} + \sigma_{ij}^{(2)}) \frac{\partial (u_i^{(1)} + u_i^{(2)})}{\partial x_j} \right] n_j d\Gamma . \tag{2.47}$$

By rearranging the terms state (1) and state (2) and the interaction terms, Equation (2.47) can be written as

$$J^{(1+2)} = J^{(1)} + J^{(2)} + M^{(1+2)} , \tag{2.48}$$

where $M^{(1+2)}$ is called the interaction integral and expressed as

$$M^{(1+2)} = \int_{\Gamma} \left(W^{(1,2)}\delta_{1j} - \sigma_{ij}^{(1)} \frac{\partial u_i^{(2)}}{\partial x_j} - \sigma_{ij}^{(2)} \frac{\partial u_i^{(1)}}{\partial x_j} \right) n_j d\Gamma , \tag{2.49}$$

in which $W^{(1,2)}$ is the interaction strain energy given by

$$W^{(1,2)} = \sigma_{ij}^{(2)} \varepsilon_{ij}^{(1)} = \sigma_{ij}^{(1)} \varepsilon_{ij}^{(2)} . \tag{2.50}$$

Using Equation (2.45), Equation (2.48) is rewritten as

$$J^{(1+2)} = J^{(1)} + J^{(2)} + \frac{2}{E_{eff}}(K_I^{(1)}K_I^{(2)} + K_{II}^{(1)}K_{II}^{(2)}) . \tag{2.51}$$

Comparing relation Equation (2.48) with Equation (2.51), the following equation is obtained

$$M^{(1+2)} = \frac{2}{E_{eff}}(K_I^{(1)}K_I^{(2)} + K_{II}^{(1)}K_{II}^{(2)}) , \tag{2.52}$$

where $M^{(1+2)}$ is the interaction integral.

It should be noted that the stress intensity factors K_I and K_{II} can easily be obtained using the above equation if only the interaction integral is obtained. Assuming that state (2) is in pure loading mode I to obtain the stress intensity factor, $K_I^{(2)} = 1$, $K_{II}^{(2)} = 0$, and Equation (2.52) is rewritten as

$$K_I^{(1)} = \frac{E_{eff}}{2} M_{\text{mode } I}^{(1)} , \tag{2.53}$$

where $M_{\text{mode } I}^{(1)}$ is the interaction integral for the case of $K_I^{(2)} = 1$, $K_{II}^{(2)} = 0$.

And, assuming that state (2) is in pure loading mode II to obtain the stress intensity factor, $K_I^{(1)} = 0$, $K_{II}^{(2)} = 1$, and Equation (2.52) is rewritten as

$$K_{II}^{(1)} = \frac{E_{eff}}{2} M_{\text{mode } II}^{(1)} , \tag{2.54}$$

where $M_{\text{mode } II}^{(1)}$ is the interaction integral for the case of $K_I^{(1)} = 0$, $K_{II}^{(2)} = 1$.

2.2.3 Domain integral form of interaction integral

Equation (2.47) and (2.49) mentioned above have the form of contour integration, which is not the most suitable form for application to the finite element method. For convenience of calculation, a process of converting the equation into a more suitable method was required, and a domain integration approach was proposed by Moran and Shih in 1987 [22]. Using divergence theorem, the J contour integral is transformed into the domain integral form and the weight function q was introduced by Combescure et al [23, 24].

As shown in Figure 2.6 the weight function is 0 in the inner contour Γ, 1 in the outer contour Γ_0, and is that linearly changes between 0 and 1 inside the domain surrounded by Γ, Γ_0, C_- and C_+. The interaction integral in Equation (2.49) is expressed as

$$M^{(1+2)} = \int_C \left(W^{(1,2)}\delta_{1j} - \sigma_{ij}^{(1)} \frac{\partial u_i^{(2)}}{\partial x_j} - \sigma_{ij}^{(2)} \frac{\partial u_i^{(1)}}{\partial x_j} \right) q m_j dC , \tag{2.55}$$

where $C = \Gamma \cup C_- \cup \Gamma_0 \cup C_+$ and $\mathbf{m}$ is the outward unit normal vector to closed path C. Note that $\mathbf{m} = -\mathbf{n}$ in the inner contour Γ and $\mathbf{m} = \mathbf{n}$ in the outer contour C_-, C_+, and Γ.

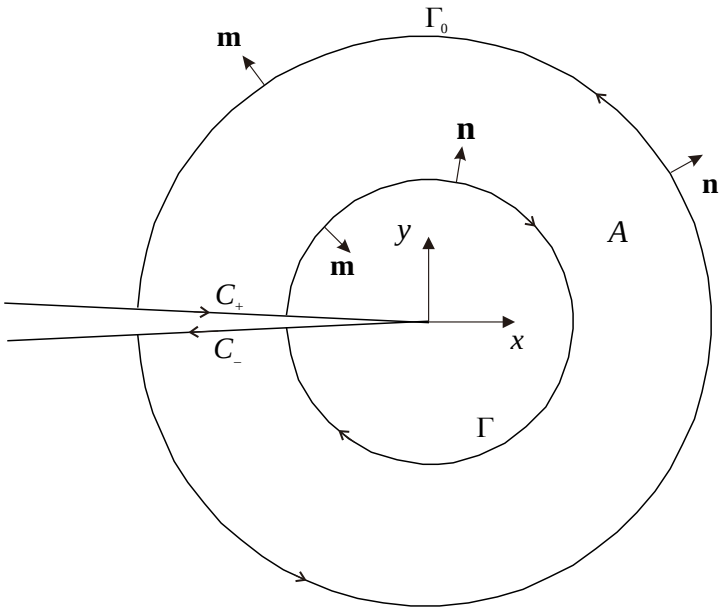

Figure 2.6 Closed domain for interaction integral

By taking the limit as Γ goes to the crack tip and assuming that crack surfaces are considered to be traction free, the interaction integrals are ready to be replaced by the domain integral form. Using divergence theorem, the interaction integrals can be written in the domain integral form as

$$M^{(1+2)} = \int_A \left(-W^{(1,2)}\delta_{1j} + \sigma_{ij}^{(1)} \frac{\partial u_i^{(2)}}{\partial x_1} + \sigma_{ij}^{(2)} \frac{\partial u_i^{(1)}}{\partial x_1} \right) \frac{\partial q}{\partial x_j} dA . \tag{2.56}$$

Chapter 3. Extended Finite Element Method

Several methods have been investigated as methods for evaluating crack propagation. Among them, dealing with the crack propagation problem using the traditional finite element method is a very cumbersome work because it requires a remesing process to meet the geometrical discontinuity. In order to improve these problems, the Extended Finite Element Method (XFEM), which was first introduced by Belytschko and Black [7] and Moës et al. [11], does not require the reconstruction of the mesh due to the propagation of the crack, and also has high accuracy. Because of these advantages, XFEM has been used in many studies to deal with cracking problems. In this chapter, we will study the basic theories about the Extended Finite Element Method.

3.1 Governing equations of cracked body

A body with outer boundary Γ and domain denoted by $\Omega \subset \mathbf{R}^2$ is considered. At the boundary Γ_t, the traction forces are applied. At the boundary surface Γ_u, the displacement boundary conditions are applied. Uniform body forces **b** are applied to the body. The outer boundary can be considered as $\Gamma = \Gamma_u \cup \Gamma_t$. In addition, the crack surface boundary denoted by Γ_d is contained in the body inside domain Ω as shown Figure 3.1. We consider that the crack boundary consists of two coincident boundaries Γ_d^+ and Γ_d^- and that there is no traction at crack boundary.

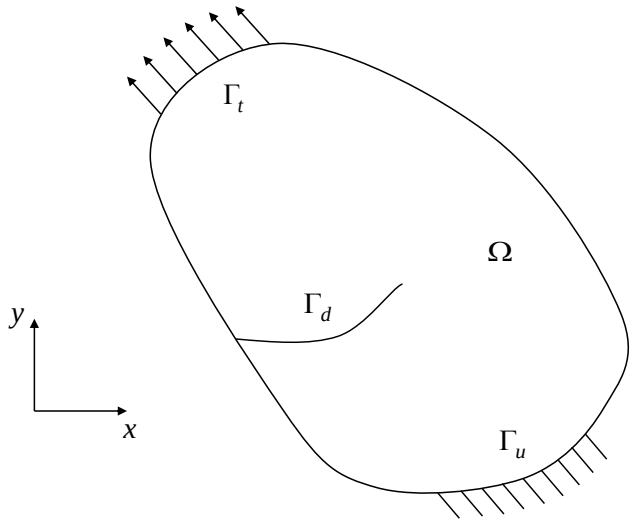

Figure 3.1 Body with a crack

The strong form of the equilibrium equation can be given by

$$\nabla \cdot \boldsymbol{\sigma} + \mathbf{b} = 0, \tag{3.1}$$

The boundary conditions for the body B can be express as

$$\boldsymbol{\sigma} \cdot \mathbf{n} = \bar{t} \quad \text{on} \quad \Gamma_t, \tag{3.2}$$

$$\boldsymbol{\sigma} \cdot \mathbf{n} = 0 \quad \text{on} \quad \Gamma_d^+, \tag{3.3}$$

$$\boldsymbol{\sigma} \cdot \mathbf{n} = 0 \quad \text{on} \quad \Gamma_d^-, \tag{3.4}$$

$$\mathbf{u} = \bar{\mathbf{u}} \quad \text{on} \quad \Gamma_u, \tag{3.5}$$

in which $\boldsymbol{\sigma}$ is the Cauchy stress tensor and $\mathbf{n}$ is the unit outward normal.

Considering the case of small displacements and small strains, strain displacement relationship can be expressed as

$$\boldsymbol{\varepsilon} = \nabla_s \mathbf{u}, \tag{3.6}$$

in which ∇_s is the symmetric components of the displacement gradient and $\boldsymbol{\varepsilon}$ is the strain tensor.

When the material is considered as a linear elastic material, the constitutive equations are given by Hook's law as

$$\boldsymbol{\sigma} = \boldsymbol{\sigma}(\boldsymbol{\varepsilon}) = \mathbf{C}\boldsymbol{\varepsilon}, \tag{3.7}$$

in which $\mathbf{C}$ is the elastic material stiffness tensor.

3.2 Partition of unity concept

Melenk and Babuška [2] have shown that traditional finite element approximations can be enriched to represent specific functions in a given domain. This is possible by using partition of unity. Because of the notion of partition of unity, all functions typically non-polynomial can be merged into the approximation of FEM. Their method can be described as follows.

The main idea is to define the sum of up to one on the domain Ω^{POU}. The partition of unity functions are given by

$$\sum_{i \in I} \phi_i = 1. \tag{3.8}$$

By multiplying any function by Equation 3.8, the following relation is obtained as

$$\sum_{i\in I}\phi_i g(x) = g(x)\,. \tag{3.9}$$

This means that any function can be reproduced when multiplied by the partition of unity functions. It also means to inherit the smoothness of the partitions of unity functions.

As shown Figure 3.2, we consider $\{\omega_i\}$, which is the system of the union of patches or clouds covering the domain Ω^{POU} centered at nodes $i \in \mathbf{I}$. A set of functions ϕ_i associated with node i of patch ω_i can be defined to have the following property.

$$\sum_{i\in I}\phi_i = 1\,. \tag{3.10}$$

Now consider g_i as the space of functions where the field $u^h\big|_{\omega_i}$ on the patch or cloud ω_i can be

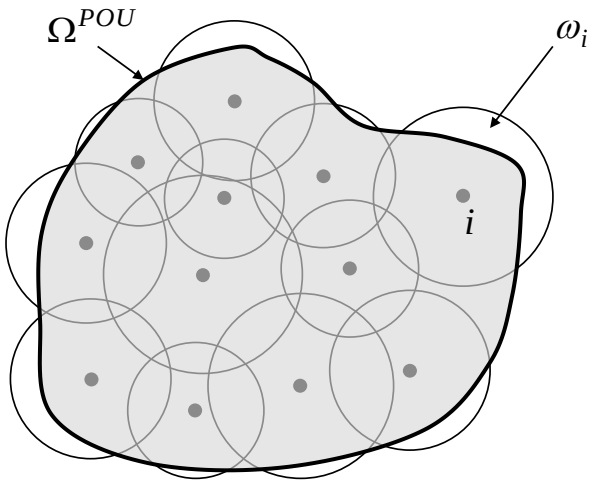

Figure 3.2 Open cover on the domain Ω^{POU} defined by clouds ω_i

well represented. Then, we can approximate the global space $U^h\big|_{\Omega}$ with G^h as follows.

$$G = \sum \phi_i g_i\,. \tag{3.11}$$

In the above discussion, the first key point about node is that the above equation has reproducibility. Second, the smoothness of the partition of unity function is inherited to the global space **G**. Third, the local property is inherited to the global space. This generally represents the advantage that any functions that are not polynomials can be accurately reproduced. This reproduced function has the smoothness of the partition of unity function.

From the viewpoint of the finite element method (FEM), it is interesting that the FE standard shape

functions can be used as partition of functions due to have the property of partition of unity. For example, the shape functions of a 4-node quadrilateral finite element are given by

$$N_1 = \frac{1}{4}(1-r)(1-s)\,. \tag{3.12}$$

$$N_2 = \frac{1}{4}(1+r)(1-s)\,. \tag{3.13}$$

$$N_3 = \frac{1}{4}(1+r)(1+s)\,. \tag{3.14}$$

$$N_4 = \frac{1}{4}(1-r)(1+s)\,. \tag{3.15}$$

in which where r and s are the coordinates in a natural coordinate system. Next, in order to define the cloud or patch, it is necessary to group all the elements that share the same node *i*. Now we can consider the union of all those elements as the cloud or patch ω_i and node *i* lies at the center of the cloud or patch ω_i. By grouping the shape functions of these elements, a partition of unity function having a boundary at zero and a unit value at node *i* is formed, which is called the subordinate of partition of unity to the cover ω_i.

Next, Duarte and Oden [14] and Melenk and Babuska [2] observed the reproducibility of the partition of unity functions as described above (Equation 3.8 and Equation 3.9). To obtain an enriched basis function, any function usually non-polynomial is multiplied with the basis function. The enriched basis functions inherit the smoothness of the partition of unity function and the property of local approximation. This relation can be express as

$$\sum \phi_i \zeta(x) = \zeta(x)\,, \tag{3.16}$$

where ϕ_i is the partition of unity shape function and $\zeta(x)$ is the enrichment function.

Now it is necessary to define the space of enrichment functions g_i. As mentioned earlier, g_i is the space of a function where $u^h\big|_{\omega_i}$ can be locally approximated on ω_i. Because of the basic properties of partition of unity, described above, we can add any functions to local approximate space. The main idea is that the local approximation space is enriched using the property of partition of unity. the enriched functional space can be defined mathematically as $\{\zeta_1(x), \zeta_2(x), \ldots, \zeta_i(x)\}$. An a priori knowledge of the properties of the expected solution (polynomial or non-polynomial functions, singular functions, trigonometric functions, Heaviside functions) can be used as local approximation function to effectively obtain a solution.

3.3 Enrichment functions for 2D crack modeling

In XFEM, by enhancing the nodal point of cut by crack elements using the enrichment function $\zeta(\mathbf{x})$, we can model the discontinuity of crack interface. In order to enhance node points, it is required to add DOF based on the discontinuity position on the domain. The displacement approximation of an enriched element can represented as

$$\mathbf{u}(\mathbf{x}) = \sum_{i\in\hat{N}} N_i(\mathbf{x})\bar{\mathbf{u}}_i + \sum_{j\in\hat{N}^{ENR}} N_j(\mathbf{x})\zeta(\mathbf{x})\bar{\mathbf{p}}_j\,, \tag{3.17}$$

in which $N(\mathbf{x})$ is the FE standard shape function and $\zeta(\mathbf{x})$ denotes the enrichment function. $\bar{\mathbf{u}}_i$ is the FE standard nodal DOF, $\hat{N}$ is the set of nodal points on the whole domain. $\bar{\mathbf{p}}_j$ is the additional nodal DOF, $\hat{N}^{ENR}$ is the set of nodal points on the domain enriched by function $\zeta(\mathbf{x})$. From Equation (3.17), the enhanced shape functions consisting of the standard terms and an enhanced terms can be expressed as

$$\mathbf{N}^{ENH} = \left[\mathbf{N}(\mathbf{x}) \quad \mathbf{N}(\mathbf{x})\zeta(\mathbf{x})\right]. \tag{3.18}$$

Taking into account the enhanced approximation of the displacement approximation in Equation (3.17), the displacement field can be obtained as

$$\mathbf{u}(\mathbf{x}_k) = \bar{\mathbf{u}}_k + \zeta(\mathbf{x}_k)\bar{\mathbf{p}}_k\,, \tag{3.19}$$

where k is a enriched node in the set $\hat{N}^{ENR}$. This displacement approximation does not correspond to the actual nodal value $\bar{\mathbf{u}}_k$ since $\zeta(\mathbf{x}_k)$ is not always zero. Therefore, the concentrated displacement approximation can be modified as

$$\mathbf{u}(\mathbf{x}) = \sum_{i\in\hat{N}} N_i(\mathbf{x})\bar{\mathbf{u}}_i + \sum_{j\in\hat{N}^{ENR}} N_j(\mathbf{x})(\zeta(\mathbf{x}) - \zeta(\mathbf{x}_j))\bar{\mathbf{p}}_j\,, \tag{3.20}$$

in which $\zeta(\mathbf{x}_j)$ is the nodal value enriched by function $\zeta(\mathbf{x})$ corresponding to j^{th} enriched node. Due to Equation (3.20), $\mathbf{u}(\mathbf{x}_k) = \bar{\mathbf{u}}_k$ is obtained. Thus, we can obtain the enriched shape functions as

$$\mathbf{N}^{ENH} = \left[\mathbf{N}(\mathbf{x}) \quad \mathbf{N}(\mathbf{x})(\zeta(\mathbf{x}) - \zeta(\mathbf{x}_i))\right]. \tag{3.21}$$

Different enrichment functions are chosen depending on the discontinuity position on the domain. In LEFM and an isotropic problem, the enrichment functions used in the cracked body generally consist of two functions, which are Heaviside function and asymptotic crack tip function.

3.3.1 Heaviside function

By using Heaviside function, it is possible to model the discontinuity, which is caused by different displacement fields on both sides of the crack. The Heaviside function is given by

$$H(\mathbf{x}) = \begin{cases} +1 & \varphi(\mathbf{x}) \geq 0 \\ -1 & \varphi(\mathbf{x}) < 0 \end{cases}, \tag{3.22}$$

in which $\varphi(\mathbf{x})$ is the signed distance function. This function $\varphi(\mathbf{x})$ is defined using the level set function. The level set function is expressed as

$$\varphi(\mathbf{x}) = \min \left\| \mathbf{x} - \mathbf{x}^* \right\| \text{sign}((\mathbf{x} - \mathbf{x}^*) \cdot \mathbf{n}_{\Gamma_d}), \tag{3.23}$$

where $\mathbf{x}^*$ is a point on the discontinuous field having the minimum distance from the point $\mathbf{x}$. $\mathbf{n}_{\Gamma_d}$ is the normal vector defined on the crack interface at the point $\mathbf{x}^*$. The Heaviside function is suitable for the modeling of cracked body due to independent displacement approximation on either sides of the crack.

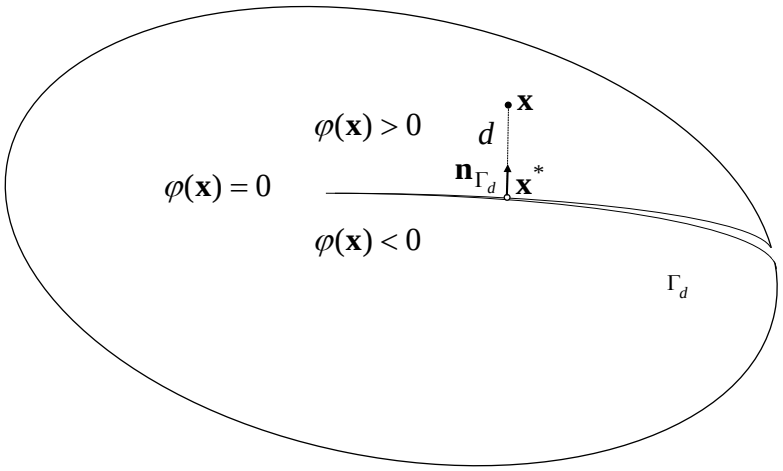

Figure 3.3 Signed distance function $\varphi(\mathbf{x})$

By applying the Heaviside function defined in Equation (3.20), we can rewrite the enriched displacement approximation for the cut by crack element in Equation (3.22) as

$$\mathbf{u}(\mathbf{x}) = \sum_{i \in \hat{N}} N_i(\mathbf{x}) \bar{\mathbf{u}}_i + \sum_{j \in \hat{N}^{DIS}} N_j(\mathbf{x})(H(\mathbf{x}) - H(\mathbf{x}_j)) \bar{\mathbf{a}}_j, \tag{3.24}$$

in which $\bar{\mathbf{a}}_j$ is the additional nodal DOF enriched by the Heaviside enrichment function, $\hat{N}$ is the set of nodal points on the whole domain and $\hat{N}^{DIS}$ is the set of nodes belong to the cut by crack element.

3.3.2 Asymptotic crack tip function

By using asymptotic functions, it is possible to model the displacement field at the region around the crack tip, which are chosen from the analytical solution given in Equation (2.21), (2.22), (2.29), (2.30), and (2.35) as

$$\begin{aligned} F(r,\theta) &= \{F_1, F_2, F_3, F_4\} \\ &= \left\{\sqrt{r}\sin\frac{\theta}{2}, \sqrt{r}\cos\frac{\theta}{2}, \sqrt{r}\sin\frac{\theta}{2}\sin\theta, \sqrt{r}\cos\frac{\theta}{2}\sin\theta\right\}, \end{aligned} \tag{3.25}$$

where $F(r,\theta)$ is the set of the asymptotic crack tip functions as shown in Figure 3.4. The first asymptotic function is used to represent the discontinuity near the crack tip on both sides of the crack. On the other hand, three other functions are used to improve the accuracy of the approximation. Therefore, the displacement approximation in Equation (3.20) enriched by the asymptotic functions in Equation (3.25) the element containing the crack tip can be rewritten as

$$\mathbf{u}(\mathbf{x}) = \sum_{i\in\hat{N}} N_i(\mathbf{x})\bar{\mathbf{u}}_i + \sum_{k\in\hat{N}^{CT}} N_k(\mathbf{x})\sum_{\gamma=1}^{4}(F_\gamma(\mathbf{x}) - F_\gamma(\mathbf{x}_k))\bar{\mathbf{b}}_k^\gamma \,, \tag{3.26}$$

in which $\bar{\mathbf{b}}_k^\gamma$ is the additional nodal DOF enriched by the asymptotic enrichment functions, $\hat{N}$ is the set of nodal points on the whole domain and $\hat{N}^{CT}$ is the set of nodes including the crack tip.

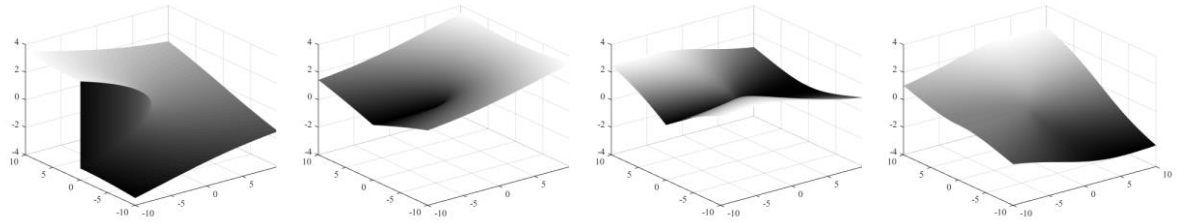

$\sqrt{r}\sin\frac{\theta}{2}$ $\sqrt{r}\cos\frac{\theta}{2}$ $\sqrt{r}\sin\frac{\theta}{2}\sin\theta,$ $\sqrt{r}\cos\frac{\theta}{2}\sin\theta$

Figure 3.4 Asymptotic crack tip functions

3.3.3 XFEM approximation

Using Equation (3.24) and (3.26), the displacement field can be obtained as

$$\mathbf{u}(\mathbf{x}) = \sum_{i\in\hat{N}} N_i(\mathbf{x})\bar{\mathbf{u}}_i + \sum_{j\in\hat{N}^{DIS}} N_j(\mathbf{x})(H(\mathbf{x}) - H(\mathbf{x}_j))\bar{\mathbf{a}}_j + \sum_{k\in\hat{N}^{CT}} N_k(\mathbf{x})\sum_{\gamma=1}^{4}(F_\gamma(\mathbf{x}) - F_\gamma(\mathbf{x}_k))\bar{\mathbf{b}}_k^\gamma \,, \tag{3.27}$$

where $\bar{\mathbf{u}}_i$ is the FE standard nodal DOF, $\bar{\mathbf{a}}_j$ is the additional nodal DOF enriched by the Heaviside enrichment

functions, $\bar{\mathbf{b}}_k^{\gamma}$ is the additional nodal DOF enriched by the asymptotic enrichment functions, $\hat{N}$ is the set of nodal points on the whole domain, $\hat{N}^{DIS}$ is the set of nodes belong to the cut by crack element, $\hat{N}^{CT}$ is the set of nodes including the crack tip. The above is detailed in Figure 3.5.

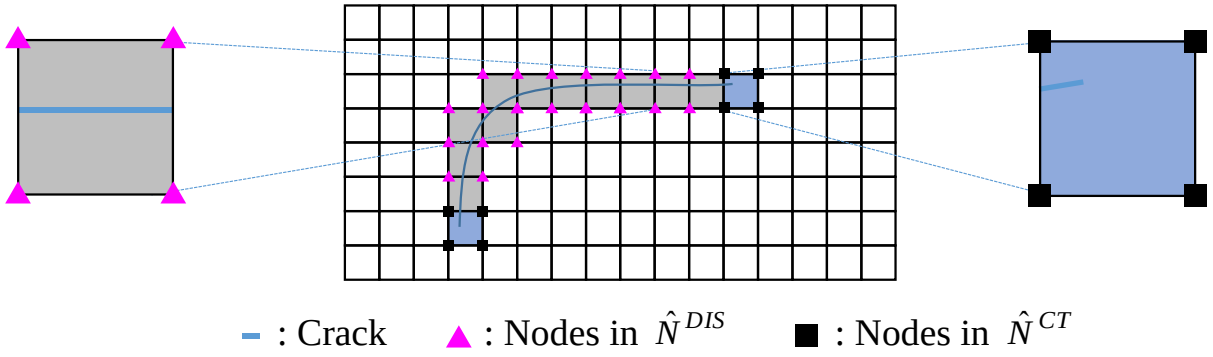

Figure 3.5 Description of enrichment strategy in XFEM

3.4 Formulation

In order to obtain the weak form of Equation (3.1), using the Galerkin method, the equilibrium equation is multiplied by the test function applicable to the domain and integrated. The test function $\delta\mathbf{u}(\mathbf{x})$ can be approximated the same as the displacement field $\mathbf{u}(\mathbf{x})$ and defined as

$$\delta\mathbf{u}(\mathbf{x}) = \mathbf{N}^{STD}(\mathbf{x})\delta\bar{\mathbf{u}} + \mathbf{N}^{H}(\mathbf{x})\delta\bar{\mathbf{a}} + \mathbf{N}^{CT}(\mathbf{x})\delta\bar{\mathbf{b}} . \tag{3.28}$$

Using the Galerkin method, the equilibrium equation in Equation (3.1) can be obtained in the form of a weak form as

$$\int_{\Omega} \delta\mathbf{u}(\mathbf{x})(\nabla\cdot\boldsymbol{\sigma} + \mathbf{b})d\Omega = 0 . \tag{3.29}$$

Being applied divergence theorem, imposed the natural boundary conditions and satisfied the traction free boundary condition on the surface of discontinuity, Equation (3.29) can be rewritten as

$$\int_{\Omega} \nabla\delta\mathbf{u} : \boldsymbol{\sigma} d\Omega + \int_{\Gamma_d} \langle\delta\mathbf{u}\rangle\boldsymbol{\sigma}\cdot\mathbf{n}_{\Gamma_d} d\Gamma = \int_{\Gamma_t} \delta\mathbf{u}\cdot\bar{\mathbf{t}} d\Gamma + \int_{\Omega} \delta\mathbf{u}\cdot\mathbf{b} d\Omega , \tag{3.30}$$

in which the symbol $\langle\ \rangle$ represents the jump across the discontinuity due to the crack. More specifically it is the difference between the corresponding value at one crack face and the corresponding value at the other opposite crack face expressed as $\langle\Phi\rangle = \Phi^{+} - \Phi^{-}$. In Equation (3.30), the second integral term on the left hand side defined

on the domain Γ_d can be removed from integral equation which imposes the traction free boundary condition ($\boldsymbol{\sigma}\cdot\mathbf{n}_{\Gamma_d}=0$ on Γ_d) and assigns the positive side and the negative side to Γ_d. As a result, Equation (3.30) can be written as

$$\begin{aligned}&-\int_{\Gamma_d^+}\delta\mathbf{u}\left(\boldsymbol{\sigma}\cdot\mathbf{n}_{\Gamma_d^+}\right)d\Gamma-\int_{\Gamma_d^-}\delta\mathbf{u}\left(\boldsymbol{\sigma}\cdot\mathbf{n}_{\Gamma_d^-}\right)d\Gamma\\&\quad=\int_{\Gamma_d}(\delta\mathbf{u}^+-\delta\mathbf{u}^-)\boldsymbol{\sigma}\cdot\mathbf{n}_{\Gamma_d}d\Gamma=\int_{\Gamma_d}\langle\delta\mathbf{u}\rangle\boldsymbol{\sigma}\cdot\mathbf{n}_{\Gamma_d}d\Gamma=0\end{aligned},\tag{3.31}$$

where $\mathbf{n}_{\Gamma_d^-}$ is the unit normal vector to Ω^-, $\mathbf{n}_{\Gamma_d^-}$ is the unity normal vector to Ω^+ descried in Figure 3.3. The superscripts – above Γ_d denotes one side of the discontinuity, the superscripts + above Γ_d denotes the other side of the discontinuity, in which $\mathbf{n}_{\Gamma_d}$ is represented as $\mathbf{n}_{\Gamma_d}=\mathbf{n}_{\Gamma_d^+}=\mathbf{n}_{\Gamma_d^-}$.

Hence, Equation (3.30) can be obtained as

$$\int_\Omega\nabla\delta\mathbf{u}:\boldsymbol{\sigma}d\Omega=\int_{\Gamma_t}\delta\mathbf{u}\cdot\bar{\mathbf{t}}d\Gamma+\int_\Omega\delta\mathbf{u}\cdot\mathbf{b}d\Omega\,.\tag{3.32}$$

Using the test function $\delta\mathbf{u}(\mathbf{x})$ in Equation (3.28) and the FE discretization, the following equation is obtained from Equation (3.32)

$$\int_\Omega\overline{\mathbf{B}}^{\mathrm{T}}\boldsymbol{\sigma}d\Omega=\int_{\Gamma_t}\overline{\mathbf{N}}^{\mathrm{T}}\bar{\mathbf{t}}d\Gamma+\int_\Omega\overline{\mathbf{N}}^{\mathrm{T}}\mathbf{b}d\Omega\,,\tag{3.33}$$

in which $\overline{\mathbf{N}}$ is defined as $\overline{\mathbf{N}}=[\mathbf{N}^{STD}\quad\mathbf{N}^{H}\quad\mathbf{N}^{CT}]$ and $\overline{\mathbf{B}}$ is defined as $\overline{\mathbf{B}}=[\mathbf{B}^{STD}\quad\mathbf{B}^{H}\quad\mathbf{B}^{CT}]$. We can obtain the system of linear equations $\mathbf{K}\overline{\mathbf{U}}-\mathbf{F}=0$ from Equation (3.33), where $\overline{\mathbf{U}}$ is the vector of nodal DOFs defined as $\overline{\mathbf{U}}=[\bar{\mathbf{u}}^{\mathrm{T}}\quad\bar{\mathbf{a}}^{\mathrm{T}}\quad\bar{\mathbf{b}}^{\mathrm{T}}]$, $\mathbf{F}$ is the vector of external force and $\mathbf{K}$ is the global stiffness matrix. Finally, the system of linear equations can be written as

$$\begin{bmatrix}\mathbf{K}_{uu}&\mathbf{K}_{ua}&\mathbf{K}_{ub}\\\mathbf{K}_{au}&\mathbf{K}_{aa}&\mathbf{K}_{ab}\\\mathbf{K}_{bu}&\mathbf{K}_{ba}&\mathbf{K}_{bb}\end{bmatrix}\begin{Bmatrix}\bar{\mathbf{u}}\\\bar{\mathbf{a}}\\\bar{\mathbf{b}}\end{Bmatrix}=\begin{Bmatrix}\mathbf{F}_u\\\mathbf{F}_a\\\mathbf{F}_b\end{Bmatrix},\tag{3.34}$$

in which $\mathbf{K}$ is the global stiffness matrix defined as

$$\mathbf{K}=\begin{bmatrix}\int_\Omega\left(\mathbf{B}^{STD}\right)^{\mathrm{T}}\mathbf{C}\mathbf{B}^{STD}d\Omega&\int_\Omega\left(\mathbf{B}^{STD}\right)^{\mathrm{T}}\mathbf{C}\mathbf{B}^{H}d\Omega&\int_\Omega\left(\mathbf{B}^{STD}\right)^{\mathrm{T}}\mathbf{C}\mathbf{B}^{CT}d\Omega\\\int_\Omega\left(\mathbf{B}^{H}\right)^{\mathrm{T}}\mathbf{C}\mathbf{B}^{STD}d\Omega&\int_\Omega\left(\mathbf{B}^{H}\right)^{\mathrm{T}}\mathbf{C}\mathbf{B}^{H}d\Omega&\int_\Omega\left(\mathbf{B}^{H}\right)^{\mathrm{T}}\mathbf{C}\mathbf{B}^{CT}d\Omega\\\int_\Omega\left(\mathbf{B}^{CT}\right)^{\mathrm{T}}\mathbf{C}\mathbf{B}^{STD}d\Omega&\int_\Omega\left(\mathbf{B}^{CT}\right)^{\mathrm{T}}\mathbf{C}\mathbf{B}^{H}d\Omega&\int_\Omega\left(\mathbf{B}^{CT}\right)^{\mathrm{T}}\mathbf{C}\mathbf{B}^{CT}d\Omega\end{bmatrix},\tag{3.35}$$

and $\mathbf{F}$ is the vector of external force defined as

$$\mathbf{F}=\begin{Bmatrix}\int_{\Gamma_t}\left(\mathbf{N}^{STD}\right)^{\mathrm{T}}\bar{\mathbf{t}}d\Gamma+\int_{\Omega}\left(\mathbf{N}^{STD}\right)^{\mathrm{T}}\mathbf{b}d\Omega\\ \int_{\Gamma_t}\left(\mathbf{N}^{H}\right)^{\mathrm{T}}\bar{\mathbf{t}}d\Gamma+\int_{\Omega}\left(\mathbf{N}^{H}\right)^{\mathrm{T}}\mathbf{b}d\Omega\\ \int_{\Gamma_t}\left(\mathbf{N}^{CT}\right)^{\mathrm{T}}\bar{\mathbf{t}}d\Gamma+\int_{\Omega}\left(\mathbf{N}^{CT}\right)^{\mathrm{T}}\mathbf{b}d\Omega\end{Bmatrix}, \tag{3.36}$$

where $\mathbf{N}_i^{STD}$ is defined as $\mathbf{N}_i^{STD}=N_i\mathbf{I}$, $\mathbf{N}_i^{H}$ is defined as $\mathbf{N}_i^{H}=N_i(H(\mathbf{x})-H(\mathbf{x}_i))\mathbf{I}$ and $\mathbf{N}_i^{CT}$ is defined as $\mathbf{N}_i^{CT}=N_i(F_\gamma(\mathbf{x})-F_\gamma(\mathbf{x}_i))\mathbf{I}$, in which $\mathbf{I}$ is a square 2×2 identity matrix. We can define the matrices $\mathbf{B}^{STD}$, $\mathbf{B}^{H}$, and $\mathbf{B}^{CT}$ for node i using the displacement field for enrichment as

$$\mathbf{B}_i^{STD}=\begin{bmatrix}\frac{\partial N_i}{\partial x} & 0\\ 0 & \frac{\partial N_i}{\partial y}\\ \frac{\partial N_i}{\partial y} & \frac{\partial N_i}{\partial x}\end{bmatrix}, \tag{3.37}$$

$$\mathbf{B}_i^{H}=\begin{bmatrix}\frac{\partial(N_i(H(\mathbf{x})-H(\mathbf{x}_i)))}{\partial x} & 0\\ 0 & \frac{\partial(N_i(H(\mathbf{x})-H(\mathbf{x}_i)))}{\partial y}\\ \frac{\partial(N_i(H(\mathbf{x})-H(\mathbf{x}_i)))}{\partial y} & \frac{\partial(N_i(H(\mathbf{x})-H(\mathbf{x}_i)))}{\partial x}\end{bmatrix}, \tag{3.38}$$

$$\mathbf{B}_i^{CT}=\begin{bmatrix}\frac{\partial(N_i(F_1(\mathbf{x})-F_1(\mathbf{x}_i)))}{\partial x} & 0 & \cdots & \frac{\partial(N_i(F_4(\mathbf{x})-F_4(\mathbf{x}_i)))}{\partial x} & 0\\ 0 & \frac{\partial(N_i(F_1(\mathbf{x})-F_1(\mathbf{x}_i)))}{\partial y} & \cdots & 0 & \frac{\partial(N_i(F_4(\mathbf{x})-F_4(\mathbf{x}_i)))}{\partial y}\\ \frac{\partial(N_i(F_1(\mathbf{x})-F_1(\mathbf{x}_i)))}{\partial y} & \frac{\partial(N_i(F_1(\mathbf{x})-F_1(\mathbf{x}_i)))}{\partial x} & & \frac{\partial(N_i(F_4(\mathbf{x})-F_4(\mathbf{x}_i)))}{\partial y} & \frac{\partial(N_i(F_4(\mathbf{x})-F_4(\mathbf{x}_i)))}{\partial x}\end{bmatrix}, \tag{3.39}$$

where the partial derivative of Heaviside functions in Equation (3.38) can be performed as

$$\frac{\partial}{\partial\mathbf{x}}(N_i(H(\mathbf{x})-H(\mathbf{x}_i)))=\frac{\partial N_i}{\partial\mathbf{x}}(H(\mathbf{x})-H(\mathbf{x}_i))+N_i\frac{\partial H(\mathbf{x})}{\partial\mathbf{x}}, \tag{3.40}$$

and the partial derivative of crack tip asymptotic functions in Equation (3.39) can be obtained as

$$\frac{\partial}{\partial\mathbf{x}}(N_i(F_\gamma(\mathbf{x})-F_\gamma(\mathbf{x}_i)))=\frac{\partial N_i}{\partial\mathbf{x}}(F_\gamma(\mathbf{x})-F_\gamma(\mathbf{x}_i))+N_i\frac{\partial F_\gamma(\mathbf{x})}{\partial\mathbf{x}}, \tag{3.41}$$

where using a transformation between Cartesian coordinate defined in a local coordinate system (x_1,x_2) and the

polar coordinate $\partial F_\gamma(\mathbf{x})/\partial \mathbf{x}$ can be represented as

$$\begin{aligned}\frac{\partial F_\gamma}{\partial x_1} &= \frac{\partial F_\gamma}{\partial r}\frac{\partial r}{\partial x_1} + \frac{\partial F_\gamma}{\partial \theta}\frac{\partial \theta}{\partial x_1} \\ \frac{\partial F_\gamma}{\partial x_2} &= \frac{\partial F_\gamma}{\partial r}\frac{\partial r}{\partial x_2} + \frac{\partial F_\gamma}{\partial \theta}\frac{\partial \theta}{\partial x_2},\end{aligned} \tag{3.42}$$

in which $\partial r/\partial x_1$ is defined as $\partial r/\partial x_1 = \cos\theta$, $\partial r/\partial x_2$ is defined as $\partial r/\partial x_2 = \sin\theta$, $\partial\theta/\partial x_1$ is defined as $\partial\theta/\partial x_1 = -\frac{1}{r}\sin\theta$ and $\partial\theta/\partial x_2$ is defined as $\partial\theta/\partial x_2 = \frac{1}{r}\cos\theta$. Using the Equations (3.42), the local partial derivatives of $F(r,\theta)$ in Equation (3.25) can be represented as

$$\begin{aligned}&\frac{\partial F_1}{\partial x_1} = -\frac{1}{2\sqrt{r}}\sin\frac{\theta}{2}, \quad \frac{\partial F_1}{\partial x_2} = -\frac{1}{2\sqrt{r}}\cos\frac{\theta}{2} \\ &\frac{\partial F_2}{\partial x_1} = -\frac{1}{2\sqrt{r}}\sin\frac{\theta}{2}, \quad \frac{\partial F_2}{\partial x_2} = -\frac{1}{2\sqrt{r}}\sin\frac{\theta}{2} \\ &\frac{\partial F_3}{\partial x_1} = -\frac{1}{2\sqrt{r}}\sin\frac{3\theta}{2}\sin\theta, \quad \frac{\partial F_3}{\partial x_2} = \frac{1}{2\sqrt{r}}\left(\sin\frac{\theta}{2} + \sin\frac{3\theta}{2}\cos\theta\right) \\ &\frac{\partial F_4}{\partial x_1} = -\frac{1}{2\sqrt{r}}\cos\frac{3\theta}{2}\sin\theta, \quad \frac{\partial F_4}{\partial x_2} = \frac{1}{2\sqrt{r}}\left(\cos\frac{\theta}{2} + \cos\frac{3\theta}{2}\cos\theta\right).\end{aligned} \tag{3.43}$$

The partial derivatives of crack tip asymptotic functions with respect to the Cartesian coordinate defined in a global coordinate system (x,y) can be given by

$$\begin{aligned}\frac{\partial F_\gamma}{\partial x} &= \frac{\partial F_\gamma}{\partial x_1}\cos\alpha - \frac{\partial F_\gamma}{\partial x_2}\sin\alpha \\ \frac{\partial F_\gamma}{\partial y} &= \frac{\partial F_\gamma}{\partial x_1}\sin\alpha + \frac{\partial F_\gamma}{\partial x_2}\cos\alpha,\end{aligned} \tag{3.44}$$

where α denotes the angle at crack tip with respect to the Cartesian coordinate defined in a global coordinate system described in Figure 3.6.

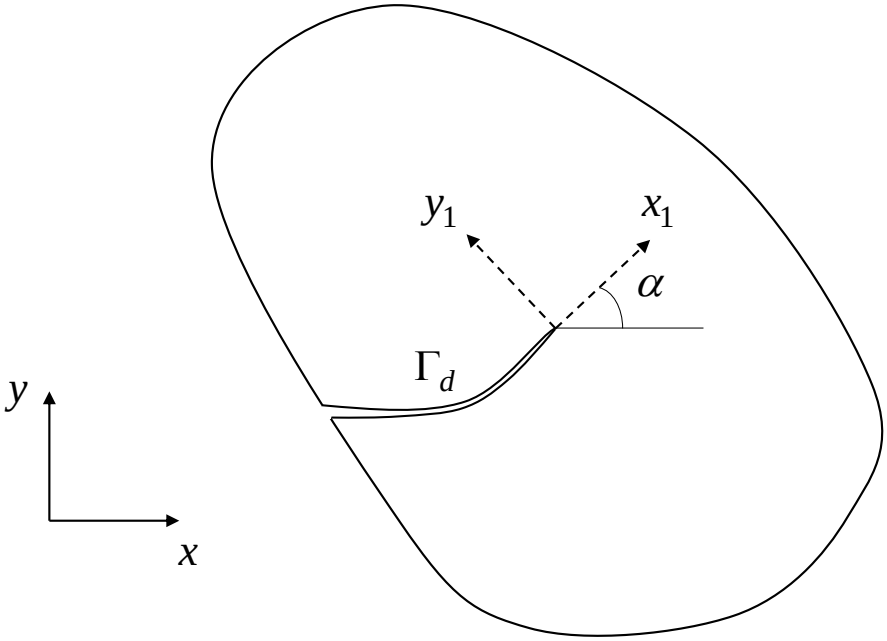

Figure 3.6 Global coordiate system and Local coordinate system at the crack tip

3.5 Numerical integration

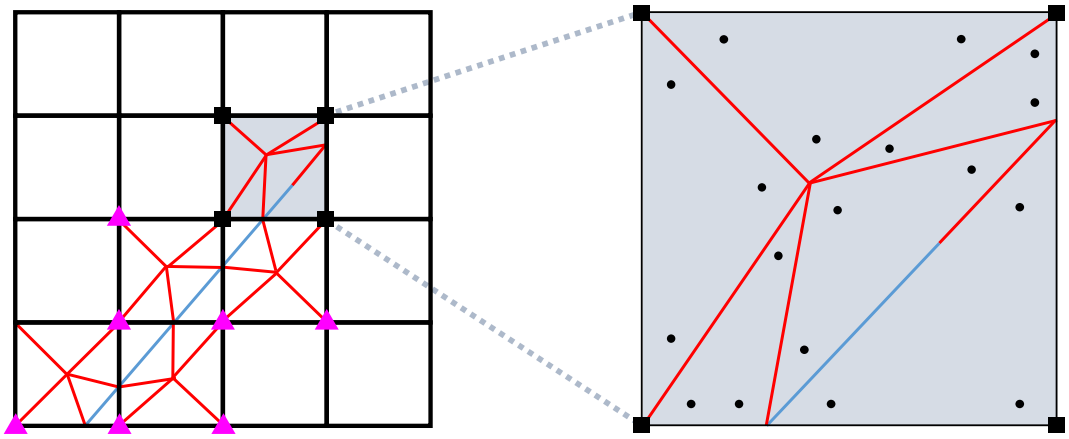

Figure 3.7 Numerical integraion for cut by crack element and crack tip element

The elements cut by crack and the elements containing a crack tip must perform a special integral. Because the field of the element cut by crack can not be accurately integrated by Gauss quadrature, the element must be partitioned so that the discontinuous field is properly integrated into both fields. As shown in Figure 3.7, the element is divided into sub-triangles that depend on the crack path, and each triangle domain is subjected to integration using Gauss quadrature.

3.6 Topological enrichment and geometrical enrichment

The enrichment schemes commonly used in XFEM are classified into topological enrichment and geometrical enrichment. As shown in Figure 3.8 (a), the way topology enforcement is applied to elements with crack tips is called topological enrichment. A method called fixed enrichment area or geometrical enrichment, which improves the convergence of topological enrichment, was proposed by Laborde et al. in 2005 [13]. The method is to apply a crack tip enticement to nodes within a specific radius that is independent of the element mesh size around the crack tip as shown in Figure 3.8 (b). Using the geometric enrichment, the convergence rate with respect to the mesh refinement is considerably improved, but the condition number of global stiffness matrix is rapidly increased to make the global stiffness matrix an ill-conditioned matrix.

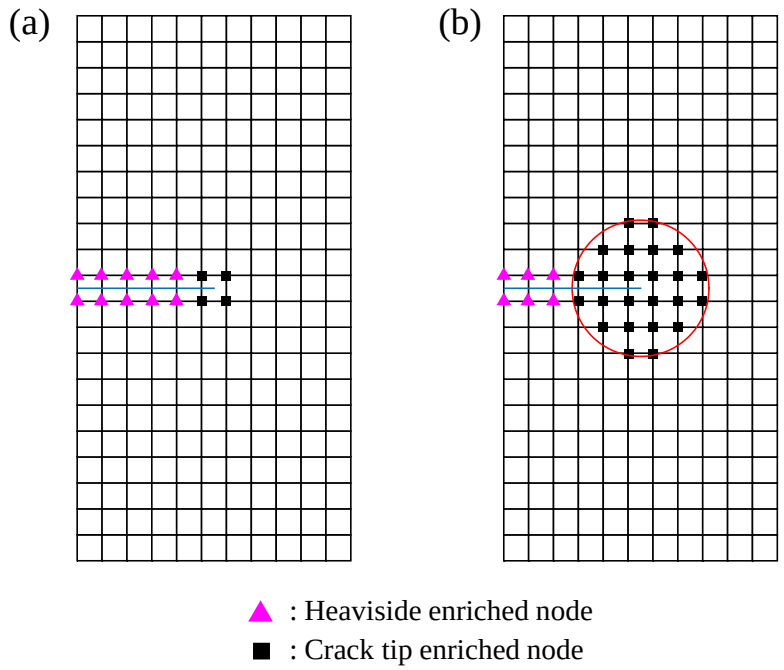

Figure 3.8 Two enrichment strategy: (a) topological enrichment, (b) geometrical enrichment

Chapter 4. Polynomial enrichment

In order to numerically analyze some objects with complex shapes, the finite element method can be effectively solved by using the concept of finite element. Because of these advantages as well as its broad applicability, the finite element method is one of the numerical method widely used in structural mechanics, fluid mechanics, electricity, nano-structures and multi-physics problems. However, mesh refinement is indispensable to obtain the desired solution accuracy when the object being analyzed has discontinuities, high gradients, or singularity. This mesh refinement requires considerable effort and in some cases requires a huge computational cost.

To solve these problems, Babuška and Melenk [2] proposed a method of enriching the solution by adding a specific enrichment function to the standard finite element method. Belytschko and Black [7] and Moës et al. [11] included enrichment functions to represent crack discontinuity. In addition, a study on improving the FE solution by applying the interpolation cover function to the standard finite element method is presented by Kim and Bathe [25], Jeon et al. [26] and Kim et al. [27]. The enriched finite element method presented by Kim and Bathe [25] and Kim et al. [27] is reviewed below. Moreover, a approach of resolving linear dependency, which was a major problem in applying the finite element methods enriched by interpolation covers to 2D solid elements, was introduced briefly [27].

4.1 Basic concept of polynomial enrichment using interpolation covers

The displacement interpolation of the 2D finite element enriched by the interpolation cover function on the cover region C_i (the union of elements sharing the node *i* shown in Figure 4.1) can be expressed as

$$\mathbf{u}(\mathbf{x}) = \sum N_i \tilde{\mathbf{u}}_i(\mathbf{x}), \tag{4.1}$$

in which N_i is the interpolation function and $\mathbf{u}_i^*(\mathbf{x})$ is given by

$$\tilde{\mathbf{u}}_i = [\tilde{u}_i \quad \tilde{v}_i]^{\mathrm{T}}, \tag{4.2}$$

where $\tilde{u}_i$ and $\tilde{v}_i$ is the interpolation covers.

The interpolation cover functions $\tilde{\mathbf{u}}_i$ defined on the cover region C_i is written as

$$\tilde{\mathbf{u}}_i = \hat{\mathbf{p}}_i(\mathbf{x})\hat{\mathbf{u}}_i, \tag{4.3}$$

where $\hat{\mathbf{p}}_i(\mathbf{x})$ and $\hat{\mathbf{u}}_i$ are a polynomial basis vector and the degree of freedom vectors for node *i* given by

$$\hat{\mathbf{u}}_i = [\hat{\mathbf{u}}_i^u \quad \hat{\mathbf{u}}_i^v]^{\mathrm{T}}, \tag{4.4}$$

$$\hat{\mathbf{u}}_i^u = [u_i^1 \quad u_i^\xi \quad u_i^\eta \quad u_i^{\xi^2} \quad u_i^{\xi\eta} \quad u_i^{\eta^2} \quad \dots \quad u_i^{\eta^p}]^{\mathrm{T}}, \tag{4.5}$$

$$\hat{\mathbf{u}}_i^v = [v_i^1 \quad v_i^\xi \quad v_i^\eta \quad v_i^{\xi^2} \quad v_i^{\xi\eta} \quad v_i^{\eta^2} \quad \dots \quad v_i^{\eta^p}]^{\mathrm{T}}, \tag{4.6}$$

$$\hat{\mathbf{p}}_i(\mathbf{x}) = [1 \quad \xi_i \quad \eta_i \quad \xi_i^2 \quad \xi_i\eta_i \quad \eta_i^2 \quad \dots \quad \eta_i^p]^{\mathrm{T}}, \tag{4.7}$$

in which $\hat{\mathbf{u}}_i^u$ and $\hat{\mathbf{u}}_i^v$ are the DOF vectors, which correspond to each basis for node *i*. (ξ_i, η_i) is the coordinate variables calculated from node *i* (shown in Figure 4.2) represented by

$$\xi_i = \frac{(x - x_i)}{\lambda_i}, \tag{4.8}$$

$$\eta_i = \frac{(y - y_i)}{\lambda_i}, \tag{4.9}$$

in which *p* is the polynomial bases degree and λ_i is the characteristic element length, which is the largest length among lengths of elements sharing node *i*.

By separating the standard FE DOF term and the additional DOF term, the displacement interpolation in Equation (5.1) can be expressed as

$$\begin{aligned} \mathbf{u} &= \bar{\mathbf{u}} + \bar{\mathbf{c}} \\ &= \sum N_i \bar{\mathbf{u}}_i + \sum \tilde{\mathbf{N}}_i \bar{\mathbf{c}}_i, \end{aligned} \tag{4.10}$$

where $\bar{\mathbf{u}}$ and $\bar{\mathbf{c}}$ are the standard nodal DOF vector and the additional nodal DOF vector given by

$$\tilde{\mathbf{N}}_i = \begin{bmatrix} \tilde{\mathbf{n}}_i & 0 \\ 0 & \tilde{\mathbf{n}}_i \end{bmatrix}, \tag{4.11}$$

$$\bar{\mathbf{c}}_i = \begin{bmatrix} \bar{\mathbf{c}}_i^u \\ \bar{\mathbf{c}}_i^v \end{bmatrix}, \tag{4.12}$$

in which $\tilde{\mathbf{N}}_i$ is the interpolation matrix, $\tilde{\mathbf{n}}_i$ is the components of the interpolation matrix $\bar{\mathbf{c}}_i^u$ is the additional nodal DOF vector corresponding to displacement *u* and $\bar{\mathbf{c}}_i^v$ is the additional nodal DOF vector corresponding to displacement *v*.

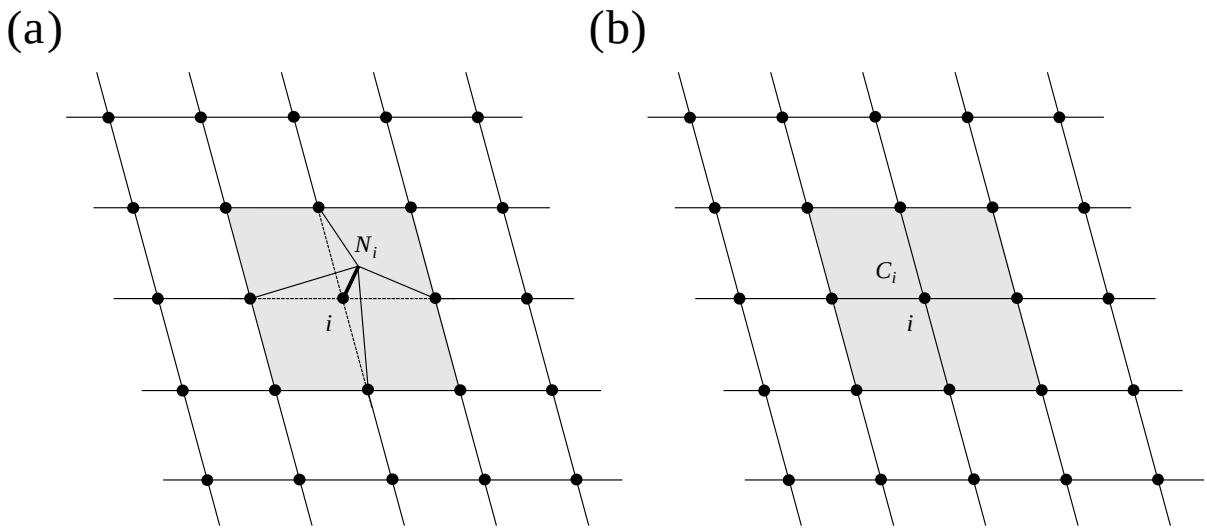

Figure 4.1 Description of cover enriched by interpolations: (a) usual bilinear interpolation function, (b) cover region C_i with node *i*.

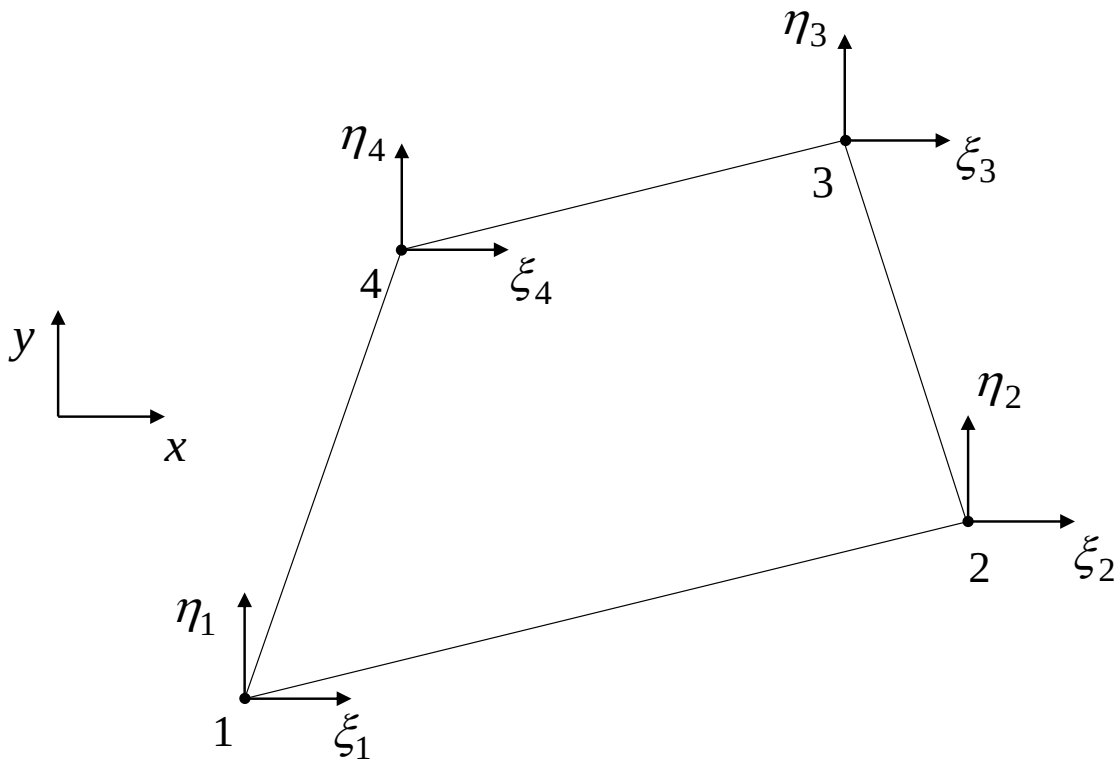

Figure 4.2 Nodal local coordiante systems (ξ_i, η_i) and global coordiante systems (x, y)

For example, in the case of $p=1$, $\tilde{\mathbf{n}}_i$ is obtained as

$$\tilde{\mathbf{n}}_i = N_i[\xi_i \quad \eta_i]\,. \tag{4.13}$$

In the case of $p=2$, $\tilde{\mathbf{n}}_i$ is obtained as

$$\tilde{\mathbf{n}}_i = N_i[\xi_i \quad \eta_i \quad \xi_i^2 \quad \xi_i\eta_i \quad \eta_i^2]\,. \tag{4.14}$$

4.1.1 Resolving linear dependence (LD) problem

When both the partition of unity function and the interpolation cover function are composed of polynomials, the linear dependence (LD) problem occurs in which the rank of the global stiffness matrix becomes insufficient even when the essential boundary conditions are appropriately applied and the solution can not be obtained. The LD problem was first observed by Babuška and Melenk in analyzing 1D problem [2]. Many researchers have made various attempts to solve the LD problem [8, 28-31]. Recently, research has been proposed to solve the LD problem and obtain a good solution by applying the piecewise linear function to the 2D 4-node quadrilateral element [27]. The polynomial enrichment technique proposed by Kim et al. [27] is applied in this paper. In this chapter, the method is reviewed.

The new shape functions were proposed to resolve the LD problem of 4-node quadrilateral elements. The 4-node quadrilateral element is divided into four triangular sub-domains, and different shape functions are applied to each sub-domain as shown Figure 4.3 (a) and (b).

For sub-domain 1, the new shape functions are obtained as

$$\hat{N}_1 = \frac{1}{4}(1+2r+s), \quad \hat{N}_2 = \frac{1}{4}(1-2r+s), \quad \hat{N}_3 = \frac{1}{4}(1-s), \quad \hat{N}_4 = \frac{1}{4}(1-s)\,. \tag{4.15}$$

For sub-domain 2, the new shape functions are obtained as

$$\hat{N}_1 = \frac{1}{4}(1+r)\,, \quad \hat{N}_2 = \frac{1}{4}(1-r+2s)\,, \quad \hat{N}_3 = \frac{1}{4}(1-r-2s)\,, \quad \hat{N}_4 = \frac{1}{4}(1+r)\,. \tag{4.16}$$

For sub-domain 3, the new shape functions are obtained as

$$\hat{N}_1 = \frac{1}{4}(1+s)\,, \quad \hat{N}_2 = \frac{1}{4}(1+s)\,, \quad \hat{N}_3 = \frac{1}{4}(1-2r-s)\,, \quad \hat{N}_4 = \frac{1}{4}(1+2r-s)\,. \tag{4.18}$$

For sub-domain 4, the new shape functions are obtained as

$$\hat{N}_1 = \frac{1}{4}(1+r+2s)\,, \quad \hat{N}_2 = \frac{1}{4}(1-r)\,, \quad \hat{N}_3 = \frac{1}{4}(1-r)\,, \quad \hat{N}_4 = \frac{1}{4}(1+r-2s)\,. \tag{4.19}$$

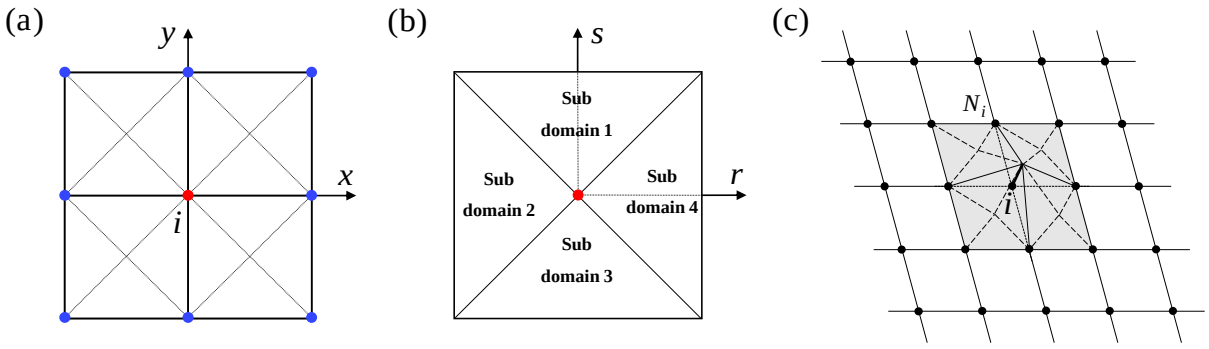

Figure 4.3 Description of the sub-domains: (a), (b) The 4-node quadrilateral elements divided into 4 triangular subdomains, (c) is the interpolation functions by piecewise linear shape functions.

The LD problem can be resolved by substituting Equations (4.15), (4.16), (4.17) and (4.18) into the bilinear shape function in Equation (4.1).

4.2 XFEM with polynomial enrichment

In chapter 4.2, the proposed polynomial enhancement technique is applied to the XFEM to improve the XFEM solution.

4.2.1 Formulation

In order to apply the polynomial enhancement technique to XFEM, Equation (3.2) is modified as

$$\mathbf{u}(\mathbf{x}) = \sum_{i\in\hat{N}} N_i(\mathbf{x})\bar{\mathbf{u}}_i + \sum_{j\in\hat{N}^{DIS}} N_j(\mathbf{x})(H(\mathbf{x})-H(\mathbf{x}_j))\bar{\mathbf{a}}_j + \sum_{k\in\hat{N}^{CT}} N_k(\mathbf{x})\sum_{\gamma=1}^{4}(F_\gamma(\mathbf{x})-F_\gamma(\mathbf{x}_k))\bar{\mathbf{b}}_k^\gamma + \sum_{l\in\hat{N}^{POL}}\tilde{\mathbf{N}}_l\bar{\mathbf{c}}_l \,, \tag{4.20}$$

where $\hat{N}$ is the set of all nodal points, $\hat{N}^{DIS}$ is the set of enriched nodes whose support is bisected by the crack, and $\hat{N}^{CT}$ is the set of nodes which include the crack tip in the support of their shape functions enriched by the asymptotic functions and $\hat{N}^{POL}$ is the set of nodes enriched by polynomial functions. In this relation, $\bar{\mathbf{u}}_i$ are the unknown standard nodal DOF at i^{th} node, $\bar{\mathbf{a}}_j$ are the unknown enriched nodal DOF associated with the

Heaviside enrichment function at node j, and $\bar{\mathbf{b}}_k^{\gamma}$ are the additional enriched nodal DOF associated with the asymptotic functions at node k, and $\bar{\mathbf{c}}_l$ are the additional enriched nodal DOF associated with the polynomial enrichment functions at node l. $\tilde{\mathbf{N}}_l$ is the interpolation matrix. $\tilde{\mathbf{N}}_l$ and $\bar{\mathbf{c}}_l$ are given by

$$\tilde{\mathbf{N}}_l = \begin{bmatrix} \tilde{\mathbf{n}}_l & 0 \\ 0 & \tilde{\mathbf{n}}_l \end{bmatrix}$$
$$\bar{\mathbf{c}}_l = \begin{bmatrix} \bar{\mathbf{c}}_l^u \\ \bar{\mathbf{c}}_l^v \end{bmatrix}, \tag{4.21}$$

where $\tilde{\mathbf{n}}_l$ is the components of the interpolation matrix and $\bar{\mathbf{c}}_i^u$ are the additional enriched nodal DOF associated with the polynomial enrichment functions at node l corresponding to displacement u and $\bar{\mathbf{c}}_i^v$ are the additional enriched nodal DOF associated with the polynomial enrichment functions at node l corresponding to displacement v. All shape functions are replaced by the shape functions given in Equation (4.15), (4.16), (4.17) and (4.18). except for the shape function corresponding to the standard DOF term. An example of applying polynomial enrichment to XFEM is depicted in Figure 4.4. (a) shows XFEM without polynomial enrichment, (b) shows XFEM with linear polynomial enrichment, and (c) shows XFEM with quadratic polynomial enrichment. As the order of polynomial enrichment increases, the number of DOF increases, but you can see that the stress jump is alleviated and the approximation is better.

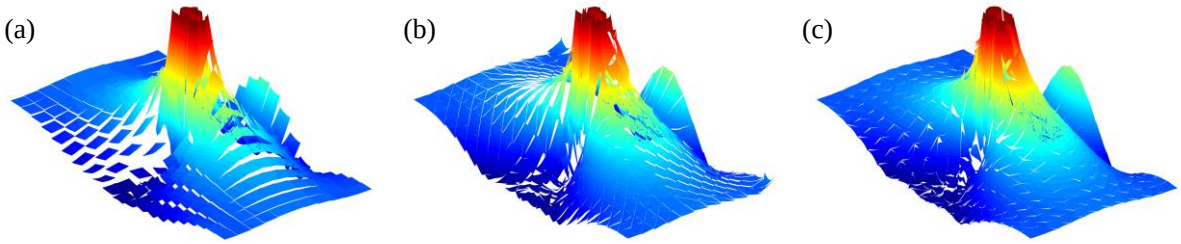

XFEM without P.E.
DOF : 577

XFEM with P.E. (p=1)
DOF : 1625

XFEM with P.E. (p=2)
DOF : 3197

Figure 4.4 Descriptions of XFEM with polynomial enrichment: (a) XFEM without polynomial enrichment, (b) XFEM with linear polynomial enrichment, (c) XFEM with quadratic polynomial enrichment

4.2.2 Numerical integration

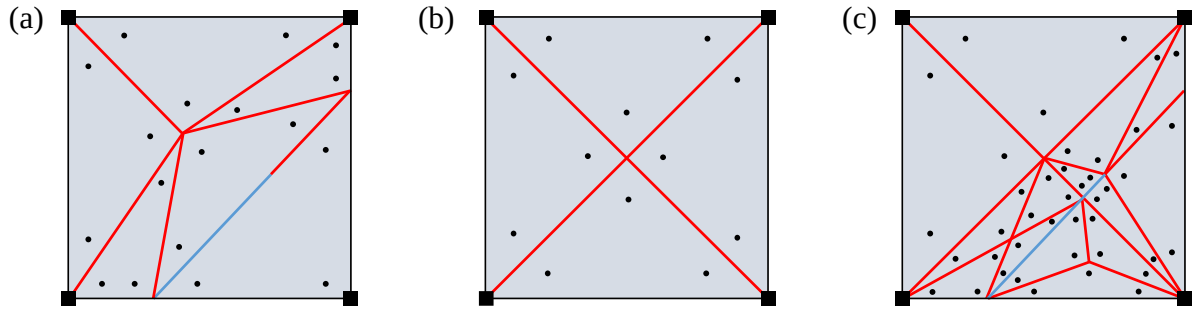

Figure 4.5 Integration schemes: (a) Integration of an element including crack tip used in XFEM, (b) Integration applied to polynomial enrichment technique, (c) Integration both techniques simultaneously

In section 3.5, the elements with discontinuous fields explained that special integration must be performed. In order to apply the polynomial enrichment technique, it is necessary to divide the sub-domains and perform the integration of the respective sub-domains. Both integration strategies must be considered simultaneously. Figure 4.5 (a) shows the integration of the elements including the crack tip from the viewpoint of the standard XFEM, and (b) shows the integration of the elements in terms of the polynomial strengthening technique. In order to simultaneously consider these two integrals, four triangular subdomains are constructed based on the center of the element as shown in (c), and then the subdomains including the crack path are reconstructed in the subdomain dependent on the crack path. Finally, integration for each subdomain is performed.

Chapter 5. Adaptive local enrichment

The adaptive mesh refinement technique improves the J-integrals to obtain the stress intensity factor numerically, but it may not be the most optimal refined mesh. Because the integration path is generally far from the crack tip, such a mesh refinement strategy may have little effect on the J-integral value. As a result, using the adaptive finite element method is strongly recommended to control the error of the J-integrals, i.e. the difference between the exact value and its approximation, and thus to obtain the optimal finite element mesh.

However, we want to improve the quality of the finite element by local enrichment strategy without using a mesh refinement strategy to obtain a better solution. Therefore, the method used in the adaptive mesh refinement strategy can be applied similarly to the adaptive enrichment strategy. In this chapter, we will study a posteriori error estimator which is used for adaptive mesh refinement strategy and propose criteria for enrichment to obtain optimal solution.

5.1 Error estimation

The solution obtained with XFEM is affected by the discretization errors associated with the size of the elements, as in FEM. Since XFEM actually tends to use discretization with coarse meshes, a tool is necessary to quantitatively evaluate the quality of these meshes. As a result, technique to estimate errors is needed in the XFEM environment.

Estimating errors in numerical computation is as important and old as numerical computation. The first paper on error estimation was first presented by Richardson [32] and reported on practical computations using finite differences. An error estimation technique considering local residuals of the numerical solution in the environment of finite element analysis was first proposed by Babuška and Rheinboldt [33]. In order to locally predict errors that occur in the energy norm, residuals that occur in the element patches or residuals that occur in a single element are investigated. There are generally two objectives in the process of error estimation. The first is to determine the error of the mesh used in the finite element, and the second is to reduce the error to an acceptable value using adaptive mesh refinement strategy.

The error estimation procedure can be generally classified into two categories: residue-based approach and recovery-based approach. Babuška and Rheinboldt [33] first proposed a residual-based method that takes into account the local residuals of the numerical solution. In order to estimate the error, the residuals in the patch of the element are calculated in terms of the energy norm. This approach has continued to be developed by other researchers. Among them, research by Ainsworth and Oden [34] was the most remarkable result. These residual-based approaches had been considered as a reliable approach among researchers for many years.

A more effective alternative to this residual-based approach is presented by Zienkiewicz and Zhu [35]. This approach uses a recovery process for more accurate error estimation. Several recovery procedures have been developed, starting with the simplest form of averaging over the nodes. These recovery-based approaches have been continually evolved by other researchers, and several recovery procedures have been proposed and attracted much attention among researchers. The basic concept of this technology is that the approximation of the error is defined by the difference between the numerical solution and the solution restored by the restoration procedure. Therefore, this approach is simple and easily applicable. Zhu and Zhang showed that there is a corresponding recovery-based process for each residual-based estimator [36], as the estimator was found to be asymptotically exact if the recovery process itself is superconvergent [37]. However, because the residual-based estimator for the recovery-based process is not always present, the error estimate with the optimal performance is more likely to be provided by the recovery method.

5.2 A posteriori error estimator

A lot of error estimators have been represented in [38], and they can be divided into two categories according to the error estimation timing. A priori error estimation provides qualitative information on convergence rate according to degrees of freedom and is based on a priori knowledge of the characteristics of solutions. A posteriori error estimation is an approach to estimate errors using a solution obtained from numerical analysis, in addition to a priori knowledge of the solution. In this approach, a quantitatively accurate measurement of the error can be provided, but a priori estimation methods can not be applied. In this paper, we use the posteriori error estimator developed by Zienkiewicz and Zhu [35] in consideration of the adaptive h-refinement procedure. This error estimator is commonly used because it is reasonably accurate despite its simplicity.

5.2.1 Zienkiewicz-Zhu error estimator

The superconvergent patch recovery (SPR) based approach is one of the most effective technique and introduced by Zienkiewicz and Zhu [37, 39]. Superconvergent patch recovery (SPR) is a method for generating very accurate recovery values, which generally has a higher convergence speed than the original solution and provides the basis for error estimation. In order to obtain the accurate and continuous stress over the entire domain with the SPR method, the nodal stresses are recovered and those nodal values are interpolated using standard FE shape functions. Using a polynomial expansion for a patch of elements which are sharing the node and fitting the raw results obtained by FE procedure at sampling points from the patch with least square technique, the nodal stress is obtained.

Before continuing, we need to define what we mean by error. This is considered to be the difference between the approximate solution and the exact solution. In the viewpoint of displacement $\mathbf{u}$, this idea can be applied and is represented as

$$\mathbf{e} = \mathbf{u} - \mathbf{u}_h , \tag{5.1}$$

where $\mathbf{u}$ is the exact solution and $\mathbf{u}_h$ is the solution obtained by FE procedure. Focusing on the strain ε or the stress σ in a similar way, the error can be given as

$$\begin{aligned} \mathbf{e}_\varepsilon &= \varepsilon - \varepsilon_h \\ \mathbf{e}_\sigma &= \sigma - \sigma_h . \end{aligned} \tag{5.2}$$

For the problems of a linear elastic material, the error of energy norm is defined as

$$\|e\| = \left[\int_\Omega (\mathbf{Be})^{\mathrm{T}} \mathbf{C} (\mathbf{Be}) d\Omega \right]^{\frac{1}{2}} , \tag{5.3}$$

in which $\mathbf{e}$ is the error in Equation (5.1) and $\mathbf{B}$ is the operator, which defines the strains as

$$\begin{aligned} \varepsilon &= \mathbf{B}\varepsilon \\ \varepsilon_h &= \mathbf{B}\varepsilon_h , \end{aligned} \tag{5.4}$$

where $\mathbf{C}$ denotes the elasticity matrix. And, the stresses is represented by

$$\begin{aligned} \sigma &= \mathbf{C}\varepsilon \\ \sigma_h &= \mathbf{C}\varepsilon_h , \end{aligned} \tag{5.5}$$

in which an initial stress and strain are ignored to simplify the problems.

Using Equation (5.4) and (5.5), the error of energy norm in Equation (5.3) can be obtained as

$$\begin{aligned} \|e\| &= \left[\int_\Omega (\varepsilon - \varepsilon_h)^{\mathrm{T}} \mathbf{C} (\varepsilon - \varepsilon_h) d\Omega \right]^{\frac{1}{2}} \\ &= \left[\int_\Omega (\varepsilon - \varepsilon_h)^{\mathrm{T}} (\sigma - \varepsilon_h) d\Omega \right]^{\frac{1}{2}} \\ &= \left[\int_\Omega (\sigma - \sigma_h)^{\mathrm{T}} \mathbf{C}^{-1} (\sigma - \sigma_h) d\Omega \right]^{\frac{1}{2}} \end{aligned} . \tag{5.6}$$

We replace σ with an improved or smoothed value that is better than the value calculated by FE procedure because the exact solution is unknown. Hence, using Equation (5.6) the following equation can be

$$\|e\| \approx \|\hat{e}\| = \left[\int_\Omega (\hat{\sigma} - \sigma_h)^{\mathrm{T}} \mathbf{C}^{-1} (\hat{\sigma} - \sigma_h) d\Omega \right]^{\frac{1}{2}} , \tag{5.7}$$

in which $\hat{\sigma}$ is the improved stress value, σ_h is the stress value obtained by FE procedure and $\|\hat{e}\|$ denotes the estimated error of energy norm. We can obtain the improved values using the stress smoothing techniques, e.g.,

nodal averaging approach [40], global smoothing technique [35, 41] and SPR technique [39]. How to improve stress values using SPR technology is explained in the next section.

And, the energy norm obtained by finite element method is given by

$$\begin{aligned} \|U_h\| &= \left[\int_\Omega {\varepsilon_h}^{\mathrm{T}} \mathbf{C} \varepsilon_h d\Omega \right]^{\frac{1}{2}} \\ &= \left[\int_\Omega {\varepsilon_h}^{\mathrm{T}} \sigma_h d\Omega \right]^{\frac{1}{2}} \\ &= \left[\int_\Omega {\sigma_h}^{\mathrm{T}} \mathbf{C}^{-1} \sigma_h d\Omega \right]^{\frac{1}{2}} . \end{aligned} \tag{5.8}$$

The above norm is defined in the whole domain. However, in terms of the contribution of each element, the norm is written as

$$\begin{aligned} \|\hat{e}\|_\Omega^2 &= \sum_{i=1}^{n} \|\hat{e}\|_i^2 \\ \|U_h\|_\Omega^2 &= \sum_{i=1}^{n} \|U_h\|_i^2 , \end{aligned} \tag{5.9}$$

where i is an element on the domain Ω and n is the total number of elements on the domain Ω. $\|U_h\|_\Omega^2$ is the energy norm on the domain Ω, $\|U_h\|_i^2$ is the energy norm of element i, $\|\hat{e}\|_\Omega^2$ the estimated error on the domain Ω, $\|\hat{e}\|_i^2$ is the estimated error of element i.

Using Equation (5.7), (5.8) and (5.9), the estimated relative error is defined as

$$\hat{\eta}_i = \frac{\|\hat{e}\|_i^2}{\sqrt{\|U_h\|_\Omega^2 + \|\hat{e}\|_\Omega^2}} . \tag{5.10}$$

5.3 Superconevergent Patch Recovery

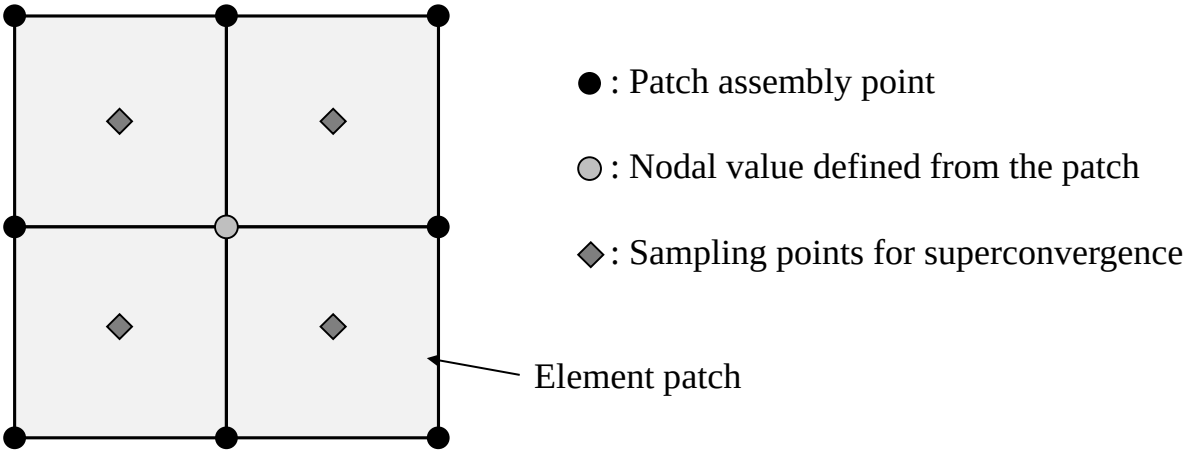

Figure 5.1 4-node elements belonging to the element patch Ω

A patch assembled around an internal vertex node is described in Figure 5.1. The figure shows rectangular elements with well defined superconvergent points.

If we take the superconvergence of σ^* at particular points k of each element, it is not difficult to calculate the $\hat{\sigma}$ that is superconvergent at every point in the element. This procedure is described in two dimensions as shown Figure 5.1, in which we must consider the internal patches (assembling all the elements at the internal node).

The values of σ^* are accurate with order p+1 at each superconvergent point. However, an approximation $\tilde{\sigma}$ can be easily obtained by a polynomial of degree p with the same order as that occurring in the shape function for displacement. When we make this polynomial fits superconvergent points using the least squares method, the accuracy of polynomial is superconvergent everywhere.

$$\tilde{\sigma}_i = \mathbf{p}(x, y)\mathbf{a}_i \,, \tag{5.11}$$

where

$$\begin{aligned} \mathbf{p}(x, y) &= [1 \quad \bar{x} \quad \bar{y} \quad \cdots \quad \bar{y}^p] \\ \mathbf{a}_i &= [a_1 \quad a_2 \quad \cdots \quad a_m]^{\mathrm{T}} \,, \end{aligned} \tag{5.12}$$

in which $\bar{x} = x - x_c$, $\bar{y} = y - y_c$ where (x_c, y_c) is the coordinates of the interior vertex node explaining the patch.

Using the least square method, a functional with *n* sampling points is minimized for each element patch,

$$\Pi = \frac{1}{2}\sum_{k=1}^{n}\left[\sigma_i^*(x_k, y_k) - \mathbf{p}_k\mathbf{a}_i\right]^2, \tag{5.13}$$

in which

$$\mathbf{p}_k = \mathbf{p}(x_k, y_k), \tag{5.14}$$

(x_k, y_k) is the coordinates of the sampling superconvergent point *k,* the coefficient $\mathbf{a}_i$ is obtained by

$$\mathbf{a}_i = \mathbf{A}^{-1}\mathbf{b}_i, \tag{5.15}$$

in which

$$\begin{aligned}\mathbf{A} &= \sum_{k=1}^{n}\mathbf{p}_k^{\mathrm{T}}\mathbf{p}_k \\ \mathbf{b}_i &= \sum_{k=1}^{n}\mathbf{p}_k^{\mathrm{T}}\sigma_i^*(x_k, y_k).\end{aligned} \tag{5.16}$$

Using $\tilde{\sigma}$, it is possible to determine the superconvergent values of $\bar{\sigma}$ at all nodes. For instance, components of the solution recovered at node a of the element patch are represented by

$$(\bar{\sigma}_i)_a = \tilde{\sigma}_i(x_a, y_a) = \mathbf{p}(x_a, y_a)\mathbf{a}_i. \tag{5.17}$$

Hence, on the assumption that the stresses recovered over the element are calculated by the same interpolation method as displacement interpolation, for recovery the nodal gradient value and the sampled stress, it is obtained as

$$\hat{\sigma} = \mathbf{N}\bar{\sigma}, \tag{5.18}$$

where $\bar{\sigma}$ is the recovered stress at the node, $\mathbf{N}$ is interpolation function and $\hat{\sigma}$ is the recovered stress interpolated by $\bar{\sigma}$.

5.4 Criteria for enrichment

The Zienkiewicz-Zhu error estimator can be used to estimate the error of each element. However, when calculating the stress intensity factor using J-integral, only the elements within a certain domain around the crack tip directly affect the stress intensity factor. The enrichment of elements on the notch or fillet with a large stress gradient except around the crack tip does not directly affect the calculation of the stress intensity factor but increases the computational cost. Therefore, the error of only the elements belonging to the local domain around

the crack tip should be estimated. Equation (5.10) is rewritten as

$$\hat{\eta}_i = \frac{\|\hat{e}\|_i^2}{\sqrt{\|U_h\|_{\Omega_L}^2 + \|\hat{e}\|_{\Omega_L}^2}}, \tag{5.19}$$

in which $\hat{\eta}_i$ is the relative error corresponding to element *i*, Ω_L is the local domain around the crack tip as shown Figure 5.2, *i* is an element on the domain Ω_L, $\|U_h\|_{\Omega_L}^2$ is the energy norm on the domain Ω_L, $\|U_h\|_i^2$ is the energy norm of element *i*, $\|\hat{e}\|_{\Omega_L}^2$ the estimated error on the domain Ω_L, $\|\hat{e}\|_i^2$ is the estimated error of element *i*.

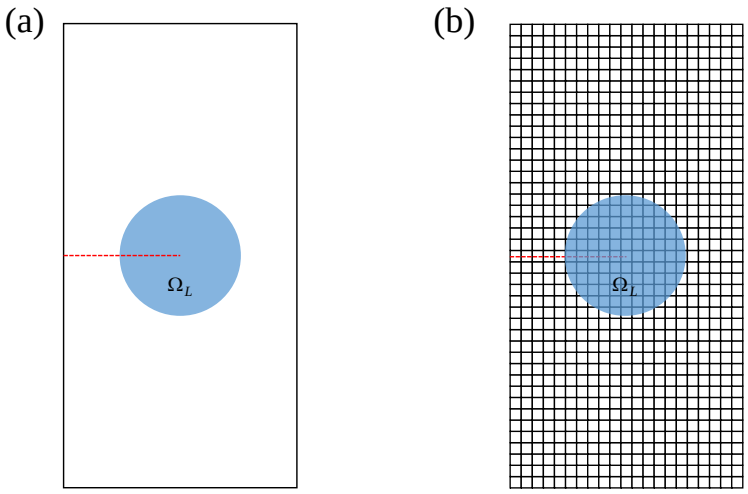

Figure 5.2 Local domain around the crack tip: (a) Local domain in crack geometry, (b) Local domian in mesh geometry

In addition, if the domain of the asymptotic crack tip enticement is larger than the domain of the J-integral, the solution becomes significantly unstable. Therefore, the size of the error estimation domain should be smaller than the J-integral domain, and only the elements on the domain Ω_L around the crack tip should be applied locally when the enriched node is adaptively selected. The order of polynomial enrichment was only linear (p = 1) and quadratic (p = 2) because the computational cost from cubic (p = 3) was too huge. Since Heaviside enrichment is excluded from adaptive enrichment because it chooses according to the crack segments, only the polynomial enrichment with linear order and quadratic order and the asymptotic crack tip enrichment are considered as adaptive enrichment. Through several tests, the following criteria for enrichment are obtained as

$$\begin{cases} 1^{st} \text{ order polynomial enriched element} & for \quad \hat{\eta}_i >= \overline{\eta}_L \\ 2^{nd} \text{ order polynomial enriched element} & for \quad \hat{\eta}_i >= \overline{\eta}_L / 3 \\ \text{Crack tip enriched element} & for \quad \hat{\eta}_i >= \overline{\eta}_L \end{cases}, \tag{5.20}$$

in which $\overline{\eta}_L$ is given by

$$\overline{\eta}_L = \frac{1}{n}\sum_{i=1}^{n} \hat{\eta}_i \,, \tag{5.21}$$

where n is the total number of elements on the domain Ω_L, $\hat{\eta}_i$ is the relative error corresponding to element i.

Examples of adaptive local enrichment is shown in Figure 5.3.

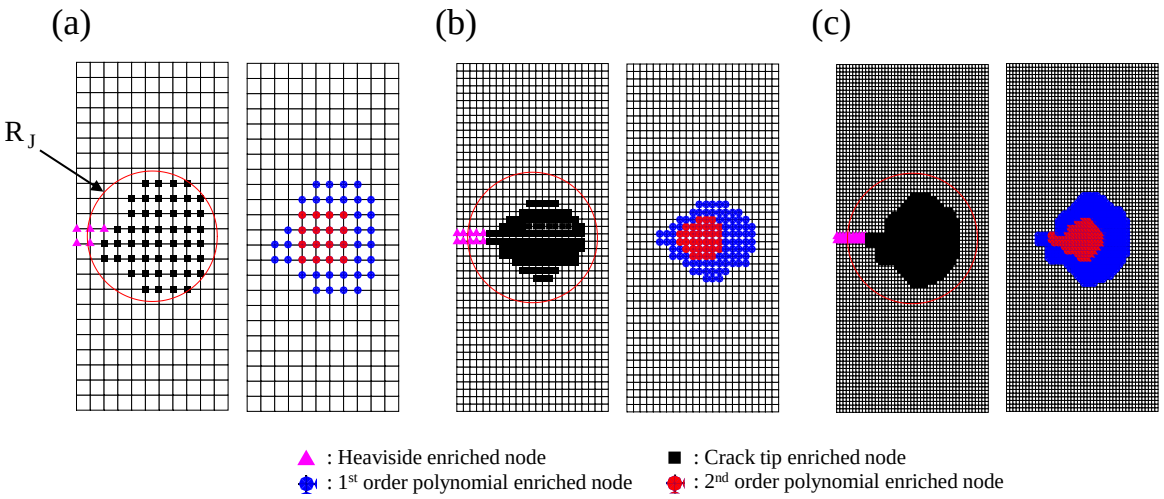

Figure 5.3 Examples for adaptive local enrichment: (a) with coarse mesh, (b) with medium mesh, (c) with fine mesh

The finite element procedure with adaptive local enrichment was performed as shown in Figure 5.4.

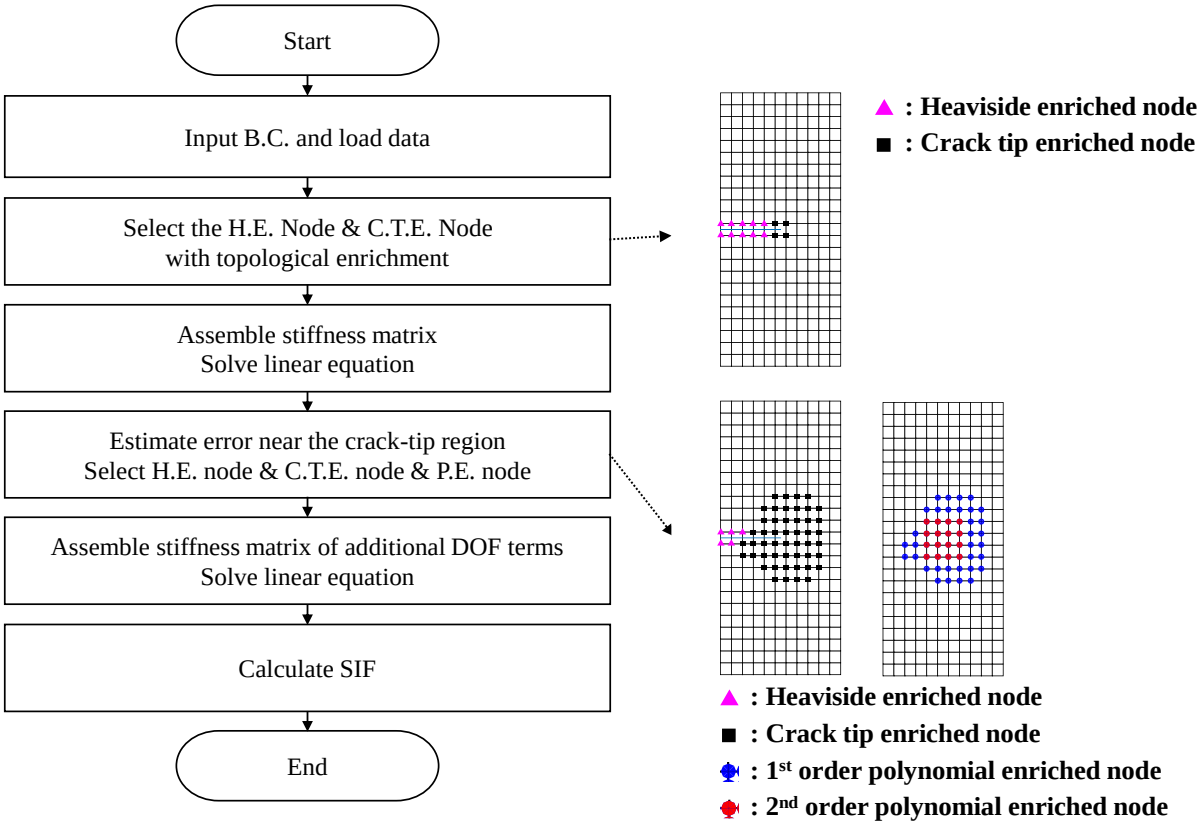

Figure 5.4 Finite element procedure for adaptive local enrichment

5.6 Convergence study

In this chapter, the proposed method is verified by solving various numerical examples by applying the above conditions. In each case, the energy relative error and the stress intensity factor relative error with respect to DOFs is compared.

The energy is written as

$$e = \int_{\Omega} \boldsymbol{\varepsilon}^{\mathrm{T}} \boldsymbol{\tau} d\Omega \quad . \tag{5.22}$$

The relative energy error is presented as

$$E_e = \frac{\left| e_{ref} - e_h \right|}{e_{ref}}, \tag{5.23}$$

where e_h is the energy obtained from FE solution, e_{ref} is the enegy obtained from FE solution using fine mesh and E_e is the relative energy error.

The relative stress intensity factor error is given by

$$E_K = \frac{\left| K_{ref} - K_h \right|}{K_{ref}}, \tag{5.24}$$

where K_h is the stress intensity factor obtained from FE solution, K_{ref} is the reference solution of the stress intensity factor and E_K is the relative stress intensity factor energy error.

5.6.1 A single edge cracked plate under uniaxial tension

A 2D single edge cracked plate under uniaxial tension shown in Figure 5.5 is considered as the first example. The height of the plate is $h = 2$, the width of the plate is $w = 2$ and the length of initial crack is $a = w/2$. The applied stress is $\sigma_0 = 1$. This example is under plane strain condition. The Young's modulus is $E = 100$, the Poisson ratio is $\nu = 0.3$ and The radius for J-integral is fixed $R_J = 0.4$. The proposed example is compared with the example applying geometrical enrichment for the three uniform rectangular mesh of 11×21, 21×41 and 41×81. Three examples with geometric enrichment radius $R_{CT} = 0.15$, $R_{CT} = 0.2$ and $R_{CT} = 0.25$ and an example applying the proposed method with an error estimation domain radius of $R_E = 0.25$ are used. The reference solution of the stress intensity factor is given by Ewalds et al. [42].

The result is given by Table 5.1 and Figure 5.6 and Figure 5.7.

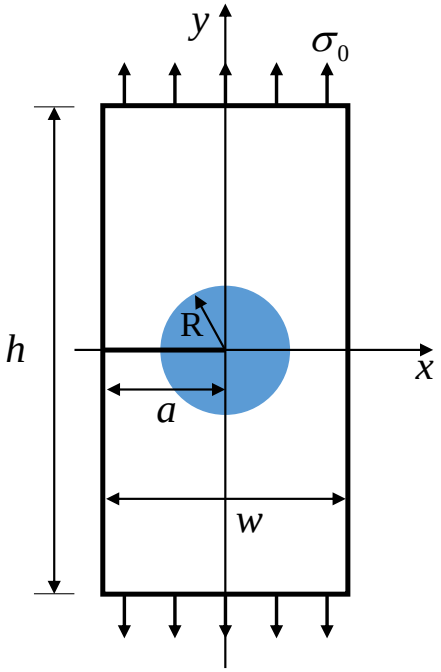

Figure 5.5 Geometry of a single edge cracked plate under uniaxial tension

Table 5.1 Results for the single edge cracked plate under uniaxial tension

Mesh		DOF	$\frac{\lvert e_{ref} - e_h \rvert}{e_{ref}} \times 100$	$\frac{\lvert K_{I\,ref} - K_{I\,h} \rvert}{K_{I\,ref}} \times 100$
11×21	$R_{CT} = 0.15$	637	3.48	3.98
	$R_{CT} = 0.2$	669	3.23	3.70
	$R_{CT} = 0.25$	729	2.54	2.96
	$R_E = 0.25$	1065	1.36	1.65
21×41	$R_{CT} = 0.15$	2133	1.13	1.30
	$R_{CT} = 0.2$	2289	0.89	1.05
	$R_{CT} = 0.25$	2573	0.72	0.86
	$R_E = 0.25$	3357	0.43	0.55
41×81	$R_{CT} = 0.15$	7905	0.28	0.36
	$R_{CT} = 0.2$	8601	0.21	0.29
	$R_{CT} = 0.25$	9585	0.17	0.24
	$R_E = 0.25$	11217	0.13	0.19

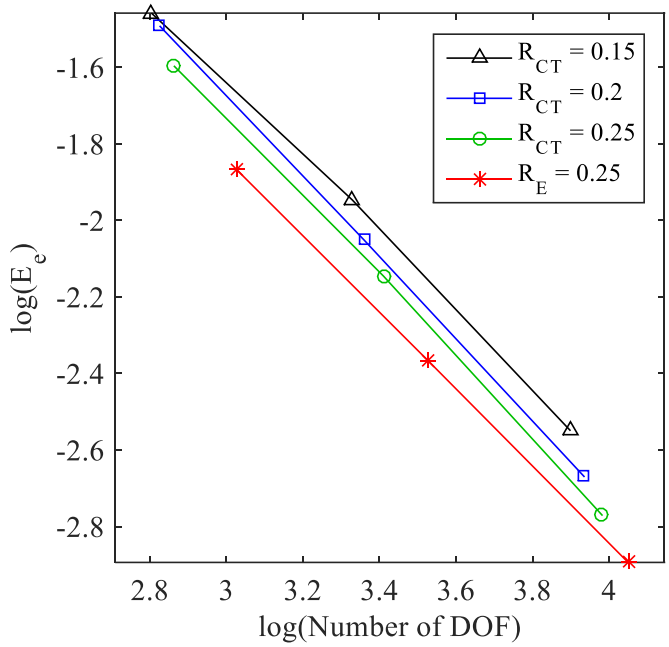

Figure 5.6 Convergence curves of the relative energy error for the single edge cracked plate under uniaxial tension with the regular meshes

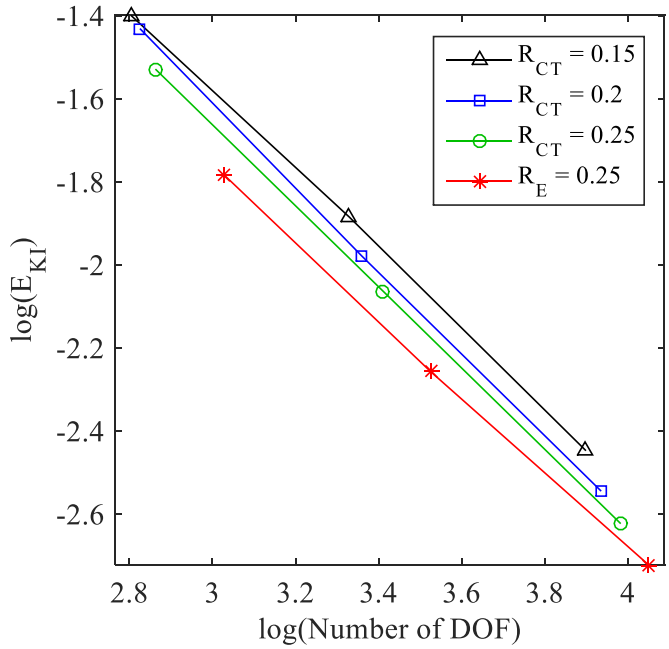

Figure 5.7 Convergence curves of the relative stress intensity factor error for the single edge cracked plate under uniaxial tension with the regular meshes

5.6.2 A single edge cracked plate under bending loading

A 2D single edge cracked plate under bending loading shown in Figure 5.8 is considered as the second example. The height of the plate is $h=12$, the width of the plate is $w=1$ and the length of initial crack is $a=w/2$. The applied stress is $\sigma_0=6$. This example is under plane strain condition. The Young's modulus is $E=1000$, the Poisson ratio is $\nu=0.3$ and The radius for J-integral is fixed $R_J=0.4$. The proposed example is compared with the example applying geometrical enrichment for the three uniform rectangular mesh of 11×121, 21×141 and 31×361. Three examples with geometric enrichment radius $R_{CT}=0.15$, $R_{CT}=0.2$ and $R_{CT}=0.25$ and an example applying the proposed method with an error estimation domain radius of $R_E=0.25$ are used. The reference solution of the stress intensity factor is given by Fett [43].

The result is given by Table 5.2 and Figure 5.9 and Figure 5.10.

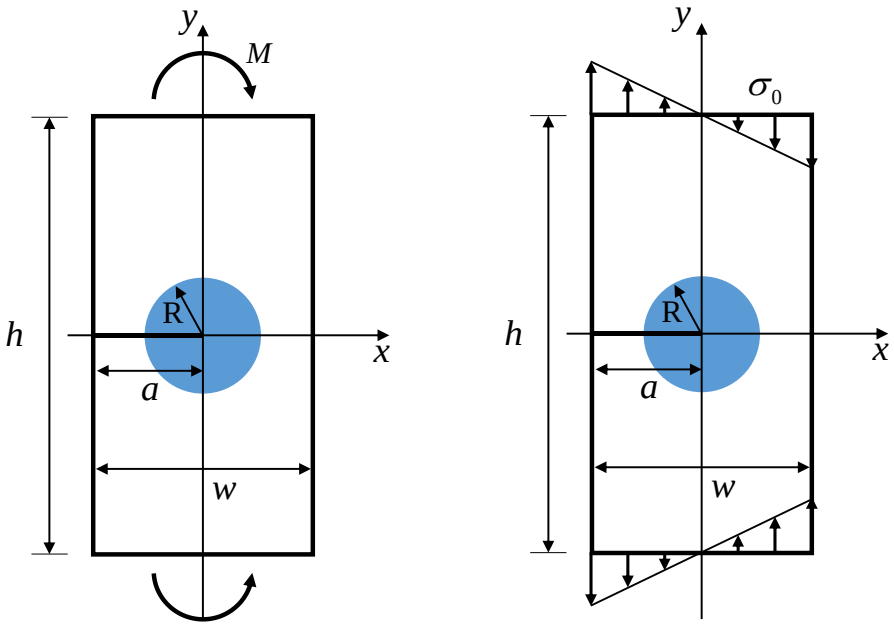

Figure 5.8 Geometry of a single edge cracked plate under bending loading

Table 5.2 Results for the single edge cracked plate under bending loading

Mesh		DOF	$\frac{\left\|e_{ref}-e_h\right\|}{e_{ref}}\times 100$	$\frac{\left\|K_{I\,ref}-K_{I\,h}\right\|}{K_{I\,ref}}\times 100$
11×121	$R_{CT}=0.15$	3004	4.41	9.06
	$R_{CT}=0.2$	3036	4.15	8.09
	$R_{CT}=0.25$	3096	3.96	7.36
	$R_E=0.25$	3476	3.46	5.49
21×241	$R_{CT}=0.15$	10932	1.17	2.35
	$R_{CT}=0.2$	11088	1.10	2.08
	$R_{CT}=0.25$	11340	1.04	1.89
	$R_E=0.25$	11812	0.95	1.55
31×361	$R_{CT}=0.15$	23720	0.51	1.00
	$R_{CT}=0.2$	24164	0.47	0.86
	$R_{CT}=0.25$	24668	0.44	0.76
	$R_E=0.25$	25868	0.41	0.63

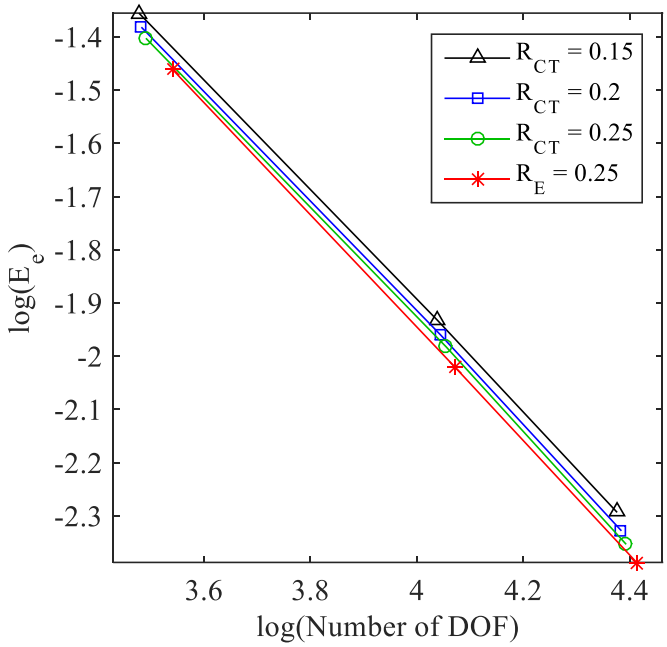

Figure 5.9 Convergence curves of the relative energy error for the single edge cracked plate under bending loading with the regular meshes

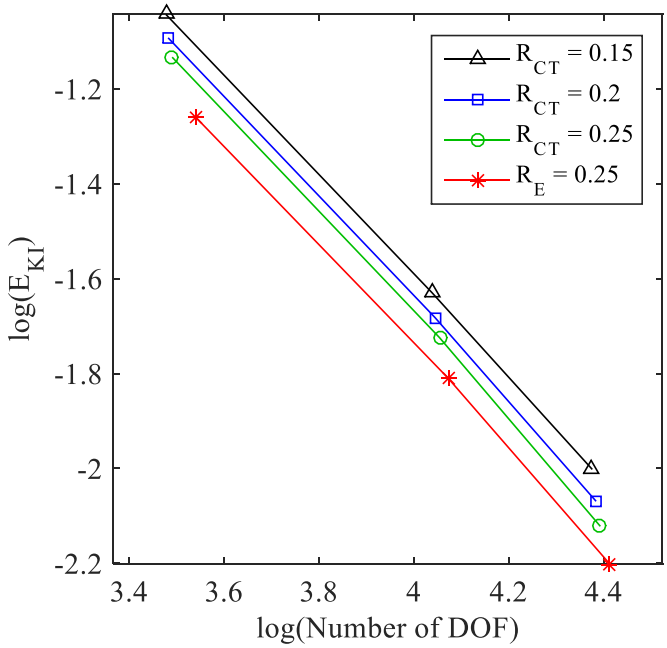

Figure 5.10 Convergence curves of the relative stress intensity factor error for the single edge cracked plate under bending loading with the regular meshes

5.6.3 A single edge cracked plate under ending shearing

A 2D single edge cracked plate under ending shearing shown in Figure 5.11 is considered as the third example. The height of the plate is $h=16$, the width of the plate is $w=7$ and the length of initial crack is $a=w/2$. The applied stress is $\sigma_0=1$. This example is under plane strain condition. The Young's modulus is $E=1000$, the Poisson ratio is $\nu=0.3$ and The radius for J-integral is fixed $R_J=3$. The proposed example is compared with the example applying geometrical enrichment for the three uniform rectangular mesh of 11×23, 23×47 and 47×95. Three examples with geometric enrichment radius $R_{CT}=1$, $R_{CT}=1.5$ and $R_{CT}=2$ and an example applying the proposed method with an error estimation domain radius of $R_E=2$ are used. The reference solution of the stress intensity factor is given by Wilson [44].

The result is given by Table 5.3 and Figure 5.12, Figure 5.13 and Figure 5.14.

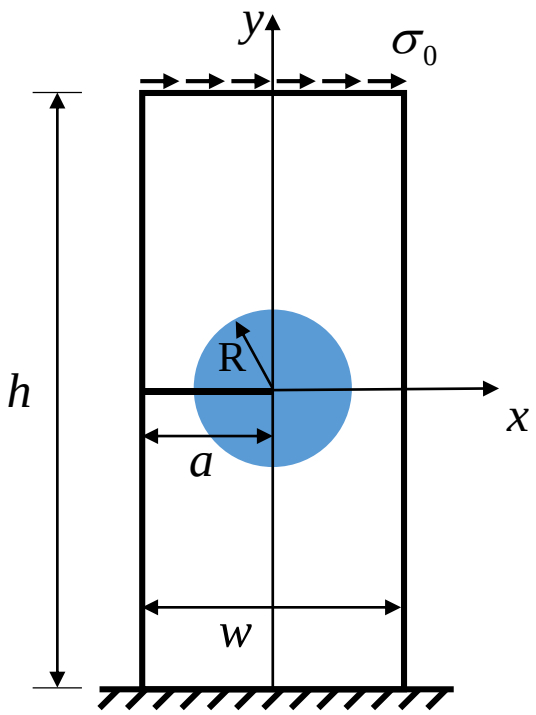

Figure 5.11 Geometry of a single edge cracked plate under ending shearing

Table 5.3 Results for the single edge cracked plate under ending shearing

Mesh		DOF	$\frac{\left\|e_{ref}-e_h\right\|}{e_{ref}}\times 100$	$\frac{\left\|K_{I\,ref}-K_{I\,h}\right\|}{K_{I\,ref}}\times 100$	$\frac{\left\|K_{II\,ref}-K_{II\,h}\right\|}{K_{II\,ref}}\times 100$
11×23	$R_{CT}=1$	604	4.55	6.56	2.24
	$R_{CT}=1.5$	696	3.17	4.33	1.64
	$R_{CT}=2$	820	2.52	3.34	1.30
	$R_E=2$	1246	1.53	1.37	0.64
23×47	$R_{CT}=1$	2548	0.98	1.26	0.73
	$R_{CT}=1.5$	2828	0.75	0.90	0.58
	$R_{CT}=2$	3236	0.61	0.67	0.51
	$R_E=2$	3806	0.47	0.45	0.45
47×95	$R_{CT}=1$	10180	0.23	0.20	0.40
	$R_{CT}=1.5$	11448	0.17	0.11	0.36
	$R_{CT}=2$	13100	0.14	0.06	0.34
	$R_E=2$	15868	0.11	0.01	0.32

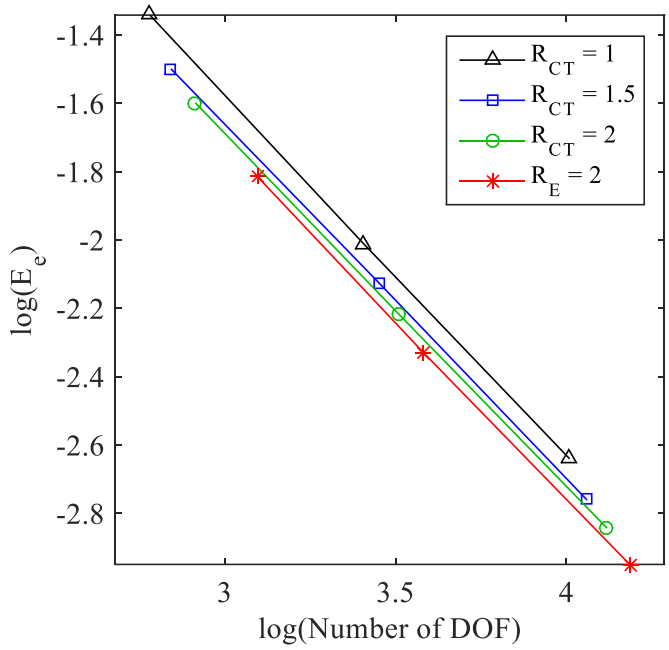

Figure 5.12 Convergence curves of the relative energy error for the single edge cracked plate under ending shearing with the regular meshes

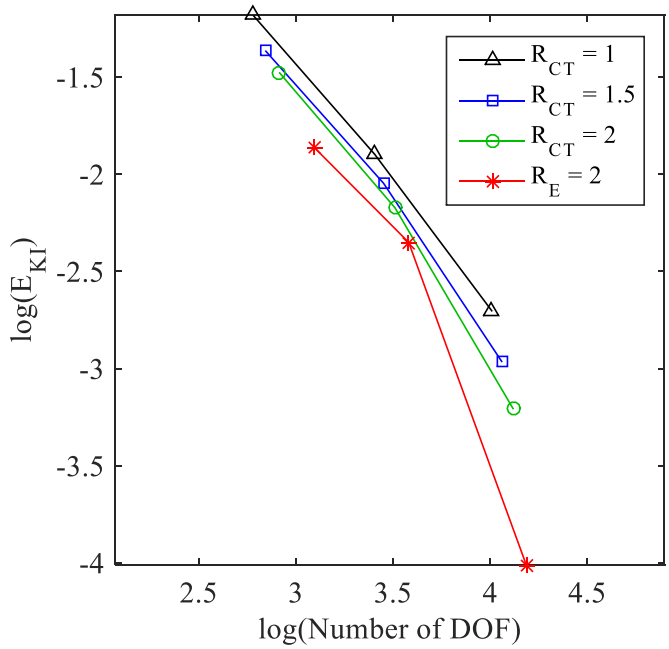

Figure 5.13 Convergence curves of the relative mode-1 stress intensity factor error for the single edge cracked plate under ending shearing with the regular meshes

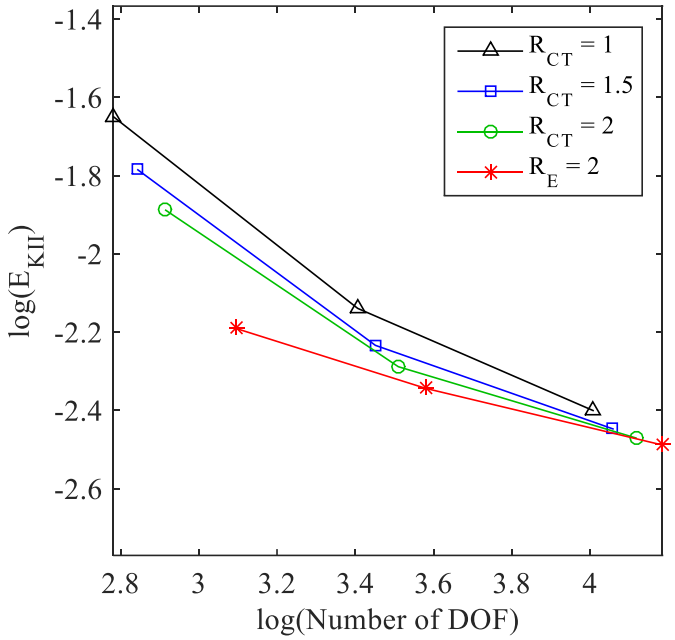

Figure 5.14 Convergence curves of the relative mode-2 stress intensity factor error for the single edge cracked plate under ending shearing with the regular meshes

Chapter 6. Conclusion

The purpose of this paper is to apply the polynomial enhancement technique to XFEM to improve the solution without mesh refinement around the crack tips. In the case of the 2D quadrilateral element, the polynomial enrichment technique was difficult due to the linear dependence problem. Recently, a research that solves the linear dependence was proposed and applied to the standard XFEM.

The proposed method can improve the solution without modifying the mesh information. However, the application of polynomial enrichment to nodes on the whole domain improve the solution results in enormous computational costs. Therefore, an adaptive enhancement concept is required, which estimates the error of each element through the Zienkiewicz-Zhu error estimator.

However, in the case of J-integral, only the elements around the crack tip are used to obtain the stress intensity factor, and enrichment of other elements causes unnecessary cost. Therefore, a concept is introduced to determine the local domain around the crack tip and to estimate only the error of the element belonging to the local domain.

In addition, error criteria is required for applying a crack tip enrichment, a first-order polynomial enrichment, and a second-order polynomial enrichment. In this study, the criteria of the adaptive local enrichment were presented using the average value for easy application in various cases. The proposed method and the XFEM were compared through several numerical examples and the efficiency was verified from the viewpoint of DOF.

Bibliography

[1] Bathe, K. J. Finite element procedures. Prentice Hall, New York. 1996.

[2] Melenk, J. M., & Babuška, I. The partition of unity finite element method: basic theory and applications. *Computer Methods in Applied Mechanics and Engineering*, 1996;139(1-4):289-314.

[3] Duarte, C. A., & Oden, J. T. An hp adaptive method using clouds. *Computer Methods in Applied Mechanics and Engineering*, 1996;139(1-4):237-262.

[4] Duarte, C. A., & Oden, J. T. Hp clouds-an hp meshless method. *Numerical Methods for Partial Differential Equations*, 1996;12(6):673-706.

[5] Griebel, M., & Schweitzer, M. A. A particle-partition of unity method for the solution of elliptic, parabolic, and hyperbolic PDEs. *SIAM Journal on Scientific Computing*, 2000;22(3):853-890.

[6] Schweitzer, M. A. Stable enrichment and local preconditioning in the particle-partition of unity method. *Numerische Mathematik*, 2011;118(1):137-170.

[7] Belytschko, T., & Black, T. Elastic crack growth in finite elements with minimal remeshing. *International Journal for Numerical Methods in Engineering*, 1999;45(5):601-620.

[8] Strouboulis, T., Babuška, I., & Copps, K. The design and analysis of the generalized finite element method. *Computer Methods in Applied Mechanics and Engineering*, 2000;181(1):43-69.

[9] Strouboulis, T., Copps, K., & Babuska, I. The generalized finite element method: an example of its implementation and illustration of its performance. *International Journal for Numerical Methods in Engineering*, 2000;47(8):1401-1417.

[10] Strouboulis, T., Copps, K., & Babuška, I. The generalized finite element method. *Computer Methods in Applied Mechanics and Engineering*, 2001;190(32):4081-4193.

[11] Moës, N., Dolbow, J., & Belytschko, T. A finite element method for crack growth without remeshing. *International Journal for Numerical Methods in Engineering*, 1999;46(1):131-150.

[12] Stazi, F. L., Budyn, E., Chessa, J., & Belytschko, T. An extended finite element method with higher-order elements for curved cracks. *Computational Mechanics*, 2003;31(1):38-48.

[13] Laborde, P., Pommier, J., Renard, Y., & Salaün, M. High-order extended finite element method for cracked domains. *International Journal for Numerical Methods in Engineering*, 2005;64(3):354-381.

[14] Béchet, É., Minnebo, H., Moës, N., & Burgardt, B. Improved implementation and robustness study of the X-FEM for stress analysis around cracks. *International Journal for Numerical Methods in Engineering*, 2005;*64(8)*:1033-1056.

[15] Anderson, T. L. Fracture mechanics: fundamentals and applications. CRC press, 2005.

[16] Griffith, A. A. The phenomena of rupture and flow in solids. *Philosophical Transactions of the Royal Society of London. Series A, containing papers of a mathematical or physical character*, 1921;221:163-198.

[17] Inglis, C. E. Stresses in a plate due to the presence of cracks and sharp corners. *Transactions of the Institute of Naval Architects*, 1913;55(219-241):193-198.

[18] Tada, H., Paris, P. C., & Irwin, G. R. The stress analysis of cracks handbook: by Hiroshi Tada, with the cooperation of Paul C. *Paris and George R. Irwin. Paris Productions & (Del Research Corp.)*, 1985.

[19] Rice, J. R. A Path Independent Integral and the Approximate Analysis of Strain Concentration by Notches and Cracks. *Journal of Applied Mechanics*, 1968;35:379-386.

[20] Yau, J. F., Wang, S. S., & Corten, H. T. A mixed-mode crack analysis of isotropic solids using conservation laws of elasticity. *Journal of Applied Mechanics*, 1980;47(2):335-341.

[21] Shih, C. F., & Asaro, R. J. Elastic-plastic analysis of cracks on bimaterial interfaces: part I—small scale yielding. *Journal of Applied Mechanics*, 1988;55(2):299-316.

[22] Moran, B., & Shih, C. F. Crack tip and associated domain integrals from momentum and energy balance. *Engineering Fracture Mechanics*, 1987;27(6):615-642.

[23] Suo, X. Z., & Combescure, A. Sur une formulation mathématique de la dérivée seconde de l'énergie potentielle en théorie de la rupture fragile. *Comptes rendus de l'Académie des sciences. Série 2, Mécanique, Physique, Chimie, Sciences de l'univers, Sciences de la Terre*, 1989;308(13):1119-1122.

[24] Suo, X. Z., & Combescure, A. Second variation of energy and an associated line independent integral in fracture mechanics. I-Theory. *European Journal of Mechanics Solids*, 1992;11:609-624.

[25] Kim, J., & Bathe, K. J The finite element method enriched by interpolation covers. *Computers & Structures*, 2013;116:35-49.

[26] Jeon, H. M., Lee, P. S., & Bathe, K. J. The MITC3 shell finite element enriched by interpolation covers. *Computers & Structures*, 2014;134:128-142.

[27] Kim, S., & Kim J.H., & Lee, P.S. Simple solution to the linear dependence problems of partition of unity-based FEM. *Proceedings of the Korea Society of Mechanical Engineering Spring Annual Meeting*, 2016;180-181.

[28] Oden, J. T., Duarte, C. A. M., & Zienkiewicz, O. C. A new cloud-based hp finite element method. *Computer Methods in Applied Mechanics and Engineering*, 1988;153(1-2):117-126.

[29] Duarte, C. A., Babuška, I., & Oden, J. T. Generalized finite element methods for three-dimensional structural mechanics problems. *Computers & Structures*, 2000;77(2):215-232.

[30] Tian, R., Yagawa, G., & Terasaka, H. Linear dependence problems of partition of unity-based generalized FEMs. *Computer Methods in Applied Mechanics and Engineering*, 2006;195(37):4768-4782.

[31] Babuška, I., & Banerjee, U. Stable generalized finite element method (SGFEM). *Computer Methods in Applied Mechanics and Engineering*, 2012;201:91-111.

[32] Richardson, L. F. The approximate arithmetical solution by finite differences of physical problems involving differential equations, with an application to the stresses in a masonry dam. *Philosophical Transactions of the Royal Society of London. Series A, Containing Papers of a Mathematical or Physical Character*, 1911;210: 307-357.

[33] Babuška, I., & Rheinboldt, W. C. A-posteriori error estimates for the finite element method. *International Journal for Numerical Methods in Engineering*, 1978;12(10):1597-1615.

[34] Ainsworth, M., & Oden, J. T. A unified approach to a posteriori error estimation using element residual methods. *Numerische Mathematik*, 1993;65(1):23-50.

[35] Zienkiewicz, O. C., & Zhu, J. Z. A simple error estimator and adaptive procedure for practical engineerng analysis. *International Journal for Numerical Methods in Engineering*, 1987;24(2):337-357.

[36] Zhu, J. Z., & Zhang, Z. The relationship of some a posteriori error estimators. *Studies in Applied Mechanics*, 1998;47:25-42.

[37] Zienkiewicz, O. C., & Zhu, J. Z. The superconvergent patch recovery and a posteriori error estimates. Part 2: Error estimates and adaptivity. *International Journal for Numerical Methods in Engineering*, 1992;33(7):1365-1382.

[38] Babuška, I., & Gui, W. Basic principles of feedback and adaptive approaches in the finite element method. *Computer Methods in Applied Mechanics and Engineering*, 1986;55(1-2):27-42.

[39] Zienkiewicz, O. C., & Zhu, J. Z. The superconvergent patch recovery and a posteriori error estimates. Part 1: The recovery technique. *International Journal for Numerical Methods in Engineering*, 1992;*33(7):1331*-1364.

[40] Byrd, D. E. Identification and elimination of errors in finite element analysis. *Ph.D. Dissertation, University of Colorado at Boudler*, 1988.

[41] Zienkiewicz, O. C., & Zhu, J. Z. Error estimates and adaptive refinement for plate bending problems. *International Journal for Numerical Methods in Engineering*, 1989;28(12):2839-2853.

[42] Ewalds, H. L., & Wanhill, R. J. H. Fracture Mechanics, Edward Arnold, London, 1984.

[43] Fett, T. T-stresses in rectangular plates and circular disks. *Engineering Fracture Mechanics*, 1998;60(5):631-652.

[44] Wilson, W. K. Combined mode fracture mechanics. *Ph.D. Dissertation, University of Pittsburgh*, 1969.